Bidirectional Brain-Machine Interfaces

for Modulating Stimulation and Neural Plasticity

Thesis by

HyeongChan Jo

In Partial Fulfillment of the Requirements for

the Degree of

Doctor of Philosophy

CALIFORNIA INSTITUTE OF TECHNOLOGY

Pasadena, California

2022

(Defended July 29, 2021)

HyeongChan Jo
ORCID: 0000-0002-1435-9124

ACKNOWLEDGEMENT

I would like to express my sincere gratitude to my advisor, Dr. Richard Andersen, for giving me the opportunity to work on these projects. His wise advice, immense knowledge, and continuous support have been always a great help for me. It was such a privilege and honor to work and study under his invaluable guidance. I would also like to thank Dr. Spencer Kellis, for his detailed guidance and friendship. He has been a great mentor for me with his patience and kindness, and has taught me many lessons both for my work and for my personal life.

In addition, I truly appreciate the hard work of my subjects, FG and EGS. Even for the most difficult and boring task, they willingly ran it without any complaints and made a lot of effort. Their patience and dedication are deeply appreciated.

I also feel sincerely grateful for all the support and help from Dr. Eberhard Fetz. Even though he lives in Seattle, he came to Pasadena from time to time to discuss my research. His enthusiasm, passion, and vast knowledge have inspired me a lot. It was such an honor to work in collaboration with him during my Ph.D.

I would also like to thank my kind committee Dr. Joel Burdick, Dr. Ueli Rutishauser, and Dr. Thanos Siapas for their time and helpful comments. Throughout the years, from candidacy to my thesis defense, their inputs have been a great help for me shaping my work.

I would like to thank the rest of my friends in the lab as well: Dr. Luke Bashford, Dr. David Bjanes, Dr. Michelle Armenta Salas, Dr. Matiar Jafari, Sarah Wandelt, and Isabelle Rosenthal for all the fun and academic discussions we had in our group meeting; Dr. Sumner Norman and Dr. Vasileios Christopoulos for helping me a lot not only for my research, but also for my career decisions; Dr. Tyson Aflalo, Dr. Jorge Gamez, Dr. Srinivas Chivukula, Dr. Sofia Sakellaridi, Dr. Carey Zhang, Whitney Griggs, Charles Guan, and Kelly Kadlec for all the great time we had in the lab. I also appreciate all the hard work done by Kelsie Pejsa and Viktor Shcherbatyuk for administrative and technical assistance.

Finally, this work would have not been possible without the support and the love of my family. I am forever grateful for it, and I dedicate this thesis to them.

ABSTRACT

In prosthetics, tactile feedback can let us feel how we interact with the environment. Without this, it is extremely difficult to perform a motor task with fine control. The same idea can be applied in the brain-machine interface (BMI), which is an interface that directly connects external devices such as prosthetic limbs to the brain. Bidirectional BMI can deliver a stimulation to the brain as a sensory feedback, which can improve the performance of motor tasks. Such a bidirectional BMI can also serve a different role, if the stimulation encodes different information: if it encodes neural activity from another brain area, for example, then bidirectional BMI can provide a bypass for a damaged neural circuit. This may also affect the neural connectivity, strengthening or weakening the underlying neural connections. In this thesis, we present experiments that explore such applications of bidirectional BMI. First, we describe an experiment for characterizing neural connectivity between different brain areas. We found neural connectivity between supramarginal gyrus (SMG) and PMv (ventral premotor area), and also between anterior intraparietal (AIP) and Brodmann's area 5 (BA5), characterized by field-field, spike-field, and partial spike-field coherence. Through partial spike-field coherence, we also revealed that the spikes in PMv may drive the activity in SMG, which is obscured in ordinary spike-field coherence. Next, we provide evidence of changes in neural connectivity caused by stimulation in S1. With spike-triggered stimulation, which delivers stimulation in S1 in response to spikes recorded in a selected channel in SMG, we could significantly increase the correlation between SMG and S1, measured by the spike time tilling coefficient (STTC) to avoid dependencies of the correlation on firing rates. Furthermore, we found that not only spike-triggered stimulations, but also random

stimulations on multiple channels in S1, can vary partial spike-field coherence in theta and alpha bands within S1; such changes mostly occurred in channel pairs with zero phase difference in partial spike-field coherence. Finally, we demonstrate the possibility of volitional control on stimulation pattern in bidirectional BMI. It is shown that the participants could not only increase or decrease a single-channel firing rate, but also hold the firing rate in a given range, demonstrating a fine control over firing rate. These findings would begin to establish a framework for closed-loop modulation of neural activity with bidirectional BMI and could be used to develop new treatments for neurological damage, such as to promote plasticity in or bridge brain areas affected by stroke.

TABLE OF CONTENTS

LIST OF ILLUSTRATIONS

Chapter 1

INTRODUCTION

Brain injury can produce deficits through the disconnection of cortical areas. Stroke in the posterior parietal cortex (PPC), for example, can lead to a variety of sensorimotor deficits including misreaching (optic ataxia), loss of online correction, and extinction/neglect (Andersen et al., 2014). When loss of function is caused by focal damage within an intermediary brain area, one possible treatment is to artificially bridge across the damaged area by recording from the input area and delivering contingent stimulation to the output area. This same kind of contingent stimulation can also be used to promote plasticity between or within brain areas (Jackson et al., 2006) for rehabilitation or treatment. Indeed, by learning to cognitively modulate neural activity at the recording site, users could even exercise control over the contingent stimulation, regulating closed-loop systems such as deep brain stimulators that otherwise require tedious manual searches over a large parameter space to deliver treatment. Devices capable of both recording and electrical stimulation of neural tissue, called bidirectional brain-machine interfaces (BMI), open a new frontier in linking fundamental principles of neuroscience to human clinical rehabilitation and treatment, whereby modulation of neural activity moves from open-loop to closed-loop—and furthermore engages cognitive processes into the closed-loop system.

These applications of bidirectional BMI are further discussed in Chapters 2, 3, and 4; before that, necessary background to understand those chapters will be provided here.

More specifically, we will discuss: 1) a brief history of BMI, 2) event-related desynchronization (ERD) and synchronization (ERS) in human electroencephalography (EEG) study, 3) neural connectivity and its quantification, and 4) cortical plasticity. Background on ERD, ERS, and neural connectivity will provide a foundation for Chapter 2 (Characterization of neural connectivity), which then can be leveraged into Chapter 3 (Promotion of cortical plasticity through spike-triggered stimulation) with additional background on cortical plasticity. Chapter 4 (Cognitive modulation of stimulation/cognitive modulation of single-channel firing rate) will build upon the concept of a traditional BMI system, to demonstrate the possibility of volitional control on bidirectional BMI.

Chapter 2

BACKGROUND

2.1. Brain-Machine Interfaces

A brain-machine interface (BMI), or a brain-computer interface (BCI), is a functional interface that directly connects the brain to external devices such as computers or prosthetic limbs. This term was first introduced by Dr. Jacques Vidal at University of California, Los Angeles, in his paper on the possibility of using electroencephalographic (EEG) signals for a communication with a computer (Vidal, 1973). Such an idea was further implemented in his following paper, which demonstrated that EEG signal can be used to control a cursor through a simple two-dimensional maze (Vidal, 1977).

Similar studies have been also conducted in animals with intracortical neural recordings. For example, in 1969, Eberhard Fetz at University of Washington showed that monkeys could learn to control the action potential firing rate of a single neuron through operant conditioning (Fetz, 1969), which was further developed into his following paper on independent control of firing rates in multiple neurons in different directions (Fetz & Baker, 1973). Another foundational study for BMI was about developing an algorithm for decoding motor intention, instead of making the animal learn how to control the neural activity. In 1989, Apostolos Georgopoulos at Johns Hopkins University successfully found a mathematical relationship between the movement direction

of the arm and the population-level neural activity recorded in a rhesus monkey's motor cortex (Georgopoulos et al., 1989).

Since then, numerous studies on BMI have built upon these foundational studies. Researchers have successfully reconstructed natural images seen by cats based on ensemble responses in the thalamus (Stanley et al., 1999), reproduced limb movements in monkeys during reaching (Wessberg et al., 2000), and further enabled the control of a robotic arm or a cursor with just brain signals in monkeys without emitting any behaviors (Carmena et al., 2003; Musallam et al., 2004; Serruya et al., 2002; Taylor et al., 2002).

Similar progress has been made in human BMI as well, thanks to intracortical recording being available for human subjects. The first BMI with intracortical recording in humans was achieved by researchers at Emory University in 1998 with a patient suffering from locked-in syndrome, demonstrating her ability to learn to control a computer cursor with her mind (Kennedy et al., 2000; Kennedy & Bakay, 1998). Since then, various other research teams have also developed invasive BMIs in human. For instance, researchers from BrainGate group at Brown University demonstrated BCI control of an artificial hand for the first time with intracortical recording from motor cortex (Hochberg et al., 2006), which was further improved in the following study from the same group (Hochberg et al., 2012) as well as another group at University of Pittsburgh (Collinger et al., 2013). Other teams include researchers at Stanford (Gilja et al., 2012; Santhanam et al., 2006), Case Western Reserve University (Ajiboye et al.,

2017), and Ohio State University (Bouton et al., 2016). There also has been an endeavor to achieve human BMI with a different recording site such as posterior parietal cortex, notably from researchers at Caltech led by Richard Andersen, to read out higher-level motor intentions (Aflalo et al., 2015).

In addition to invasive BMIs, partially invasive BMIs and non-invasive BMIs have been also developed and explored in human subjects. BMI with electrocorticography (ECoG), for example, is considered to be partially invasive since the electrodes rest on the brain rather than within the gray matter, although it requires craniotomy to implant the electrodes inside the skull. The first human BMI using ECoG was developed in 2004 by researchers at Washington University led by Eric Leuthardt, which showed volitional control of two-dimensional movement of a computer cursor in multiple subjects (Schalk et al., 2008). Along with other studies (Milekovic et al., 2012; Pistohl et al., 2008, 2012; Yanagisawa et al., 2012), the success of ECoG-based BMI suggests the possibility of using it for clinical applications.

Non-invasive BMIs, especially EEG-based BMIs, also have advantages and disadvantages. Their clear advantage is that they do not require any surgery, which makes it much easier for the subjects to participate, compared to other invasive and partially invasive methods. However, they suffer from relatively poor spatial resolution, and the effective frequency range is limited since the skull dampens high-frequency signals. Nevertheless, researchers in a number of labs have successfully demonstrated the efficacy of EEG-based BMI. For

example, Jonathan Wolpaw and his colleagues have shown EEG-based BMI for cursor control in 1991 (Wolpaw et al., 1991), and further demonstrated its performance on three-dimensional control (McFarland et al., 2010). Bin He and his research team at the University of Minnesota have also shown participants' ability to control a virtual helicopter in three-dimensional space with motor imagery (Doud et al., 2011), and further developed this study into controlling an actual robotic quadcopter with EEG signals (LaFleur et al., 2013). Upper-limb and lower-limb exoskeletons have been also recently developed using EEG-based BMI, by Jose L. Contreras-Vidal and his research team at University of Houston (Bhagat et al., 2016; He et al., 2018)

Although we have mainly focused on BMI for reading out neural signals, BMIs can also stimulate the brain. For example, brain implants delivering electrical stimulation on the occipital cortex can produce phosphenes, which refer to the phenomenon of seeing light by electrically stimulating visual cortex (Dobelle & Mladejovsky, 1974). BMIs can also deliver stimulation to the somatosensory cortex for a motor BMI to elicit somatosensory percepts (O'Doherty et al., 2011). In addition to substituting a missing sensory modality, studies also have shown that neural stimulation can modify, or restore, functional connectivity (Miranda et al., 2015), which has been shown with transcranial magnetic stimulation (Jacobs et al., 2012), direct current stimulation (Rahman et al., 2013), and also with spike-triggered microstimulation (Jackson et al., 2006; Song et al., 2013). This demonstrates the possibility of using electrical stimulation for the treatment

of a traumatic brain injury or neurological diseases, such as stroke, as shown in rodents (Guggenmos et al., 2013) and monkeys (Khanna et al., 2021).

Nowadays, a number of companies is also interested in developing BMIs. Big tech companies such as Facebook and Microsoft have been conducting BMI research for the past few years, and start-ups like Kernel and MindX have also been developing their own BMI systems, publishing several papers and conference proceedings on the subject (Ban et al., 2021). Recently, the CEO of Tesla, Elon Musk, announced he would begin developing neural interface for humans in his company Neuralink, drawing people's attention to the field of BMI. This shows the possibility of a commercialized BMI system in the market, hopefully in the near future.

2.2. Event-related desynchronization/synchronization

Neural oscillation refers to any rhythmic or repetitive neural activity found in a neural tissue, which has been observed as early as 1890 by a researcher Adolf Beck, who found rhythmic oscillations caused by light in the brains of rabbits and dogs (Coenen et al., 2014). Neural oscillation can occur in a microscopic level where individual neurons show oscillations in membrane potentials or in firing patterns, but it can also happen in a much larger scale that can be observed by EEG, ECoG, or magnetoencephalography (MEG). Such a large-scale

oscillation can be caused by a synchronized firing activity of a group of neurons, which generally arises from feedback connections between the neurons.

The synchronized activity of neural ensembles can change during different behavioral tasks, such as receiving external stimuli or preparing movements, which leads to changes in the amplitude of the oscillation: if the activity becomes more synchronized, the amplitude will increase; if the activity gets less synchronized, the amplitude will decrease. For example, auditory stimuli can increase the gamma activity around 40Hz in auditory cortex, measured in EEG and MEG (Pantev et al., 1991; Tallon-Baudry & Bertrand, 1999). Since its basis is the synchronization of the neural activity in the ensemble evoked by a specific event (such as the onset of sensory stimuli), increases and decreases in the amplitude of a neural oscillation are called event-related synchronization (ERS) and event-related desynchronization (ERD), respectively (Pfurtscheller & Lopes da Silva, 1999).

One great example of ERS and ERD can be seen in sensorimotor rhythm (SMR). SMR is a neural oscillation observable in the sensorimotor cortex, whose frequency is usually in the range of 13 to 15 Hz (Arroyo et al., 1993), although it can be lower or higher than this (Pfurtscheller & McFarland, 2012). SMR? can be found when a person does not move, but during motor outputs, motor preparation (Pfurtscheller & Aranibar, 1979), and even motor imagery (Henry, 2006), its amplitude typically decreases, which is an example of ERD. There are different interpretations for this, such as SMR representing epiphenomenal

background rhythmic activity in a neuronal population that can be disrupted during movement (Chen et al., 1998; Cheyne, 2013; Pfurtscheller et al., 1996), or SMR suppressing task-irrelevant activity (Pineda, 2005; Zabielska-Mendyk et al., 2018; Zapała et al., 2020). It can also increase at the completion of the movement, which is an example of ERS (Pfurtscheller, 1992).

2.3. Neural connectivity and its quantification

Neural connectivity, or brain connectivity, is patterns of links in the brain (Sporns, 2007). It can be identified by an anatomical structure, which leads to structural connectivity, or by statistical dependency of the signal, which defines functional connectivity (Sporns, 2007).

As the name implies, we need to have a map of neurons and their axonal projections to obtain structural connectivity. This can be done through cytoarchitectural studies where brain tissues are sliced and examined under a microscope, or through tract-tracing experiments that can identify axonal projects from one brain area to another (Zamora-López et al., 2011). Both of these methods, however, are destructive and invasive, which limits their usage in human subjects. On the other hand, diffusion tensor imaging or DTI (Basser, 1995) is a noninvasive method, which makes it one of the most widely-used methods to explore structural connectivity in the human brain (Basser et al., 2000) despite its low resolution compared to tract-tracing and histological study.

DTI measures the diffusion of water molecules in tissue. Due to the physical constraints of the neuroanatomical structure, following the diffusion-driven displacements of the water molecules in the brain provides information about its anatomical structure (Le Bihan et al., 2001). There are some technical limitations with DTI such as the difficulty to distinguish the axonal fibers running parallel to each other from the ones crossing each other (Zamora-López et al., 2011), but it can still provide a large-scale structural connectivity in a living brain (Hagmann et al., 2008; Sporns et al., 2005; Zamora-López et al., 2011).

In contrast, functional connectivity refers to patterns of statistical association between neural activity in different brain regions (Colombo & Weinberger, 2018). Therefore, it is about the temporal relationship between signals, rather than the actual structural connections. The two primary types of electrophysiological data for analyzing functional connectivity are spikes and local field potentials (LFPs). Oscillations in LFPs represent synchronized excitability of local neurons (Buzsáki & Wang, 2012), and when such oscillations are synchronized between two brain regions, they may facilitate information flow between those regions (Womelsdorf et al., 2007). Spikes, on the other hand, reflect neural information transmitted from one brain area to another, which can help establish long-range synchronization (Wang, 2010). Lastly, the synchronization between LFP and spikes can provide an indirect measure of the relationship between the outputs of a region (spikes) and the synaptic inputs of a region (LFP) (Harvey et al., 2009; Okun et al., 2010; Vinck et al., 2012). Hence,

the synchrony with spikes, within LFPs, or between spikes and LFPs can serve as a metric for functional connectivity (Bastos & Schoffelen, 2016).

There are several subdivisions of methods for quantifying neural connectivity through the synchrony in the signals: time domain vs. frequency domain, directed vs. non-directed, and model-based vs. model-free (Bastos & Schoffelen, 2016). Time domain- and frequency domain-based methods can be differentiated based on how the signals are compared. If you want to see how the signals change in time to compare them and evaluate the neural connectivity, then you can use the signals as is, which is a time-domain approach; if you want to examine each of the frequency components of the signals and investigate their interactions, then it is more appropriate to represent the signals in frequency domain before comparison, which is a frequency-domain approach. Directed and non-directed metrics differ in whether they quantify causal relationships between signals. Granger causality and transfer entropy, for example, examine the causal relationship based on whether one signal can in some way predict the other signal (Bastos & Schoffelen, 2016). Non-directed metrics, on the other hand, do not provide any information on direction of influence. Lastly, model-based metrics build upon an assumption of a linear relationship between the signals, as in the Pearson correlation coefficient, whereas model-free measures provide a more generalized approach, which includes both linear and non-linear interactions. Although there are many metrics for quantification of neural connectivity, we are going to focus on coherence and spike correlation in this chapter, since they are

the methods used in the study. We chose these two model-based metrics because we wanted to capture the interactions between spikes and oscillations at similar frequencies. There might be interesting non-linear relationships as well, such as cross-frequency coupling, but the interaction between oscillations at similar frequency would be a good starting point.

Spike correlation is a time-domain, non-directed, model-based approach for functional connectivity, and it measures the degree of correlation between neural spike trains. Highly correlated activities can arise from direct synaptic connections or shared presynaptic partners (Tchumatchenko et al., 2011), so spike correlation has been used as a key analysis of neural data in many systems (Chiappalone et al., 2006; Cutts & Eglen, 2014; Dehorter et al., 2012; Kirkby et al., 2013). The Pearson correlation coefficient is the simplest measure of spike correlation, and it quantifies the linear relationship between two time series. However, since spikes can be sparse, inadequate size of the windows for quantifying firing rate can result in a misleading Pearson correlation coefficient, as periods with no spikes should not count as correlated (Cutts & Eglen, 2014). Correlation index (Wong et al., 1993) is one of the alternatives for Pearson correlation coefficient which has a widespread usage (MacLaren et al., 2011; Personius et al., 2007), but it still suffers due to the bias from firing rates and firing patterns (Cutts & Eglen, 2014).

One alternative to correlation index, which removes the bias from firing rates and patterns, is spike time tiling coefficient (STTC) (Cutts & Eglen, 2014). The formula for computing STTC between spikes from areas A and B is as follows:

$$STTC = \frac{1}{2}\left(\frac{P_A - P_B}{1 - P_A T_B} + \frac{P_B - P_A}{1 - P_B T_A}\right).$$

Here, P_A stands for the proportion of the spikes in A that falls within ±Δt of any spikes in B, and vice versa for P_B. T_A and T_B are the proportion of the total time that falls within ±Δt of any spikes in A and B, respectively. Because STTC looks into the proportion of spikes from one area that lies within ±Δt of any spikes in the other area, it is insensitive to firing rate. It also accounts for the amount of correlation expected by chance based on the proportion of total recording time that falls into those time windows.

Coherence, on the other hand, is a frequency-domain, non-directed, model-based method for quantifying functional connectivity. It is a frequency domain equivalent to cross-correlation, which is a time-domain estimate of the signals' interactions, and its squared value quantifies how much variance in one signal can be explained by the other, and vice versa (Cutts & Eglen, 2014). The formula for the coherence between signal x and y is as follows:

$$coh_{xy}(\omega) = \frac{|S_{xy}(\omega)|}{\sqrt{S_{xx}(\omega)\, S_{yy}(\omega)}}.$$

Here, S_{xy} is the cross-spectral density between x and y, whereas S_{xx} and S_{yy} are the auto spectral density in signal x and y, respectively. As a function of frequency, this equation quantifies the phase synchrony between x and y, which can be either spikes or LFPs. For example, spike data can be represented as zeros and ones, which then can be converted into frequency domain representation in the same manner we handle the LFP data. If both of the signals are LFPs, then it is called field-field coherence, and if one of them is spike train and the other is LFP, then it is referred to as spike-field coherence. It can be both spikes as well, which leads to spike-spike coherence.

High field-field coherence across different brain regions indicates that the neural population in one area is active at the same time, or in a time-locked fashion, with the population in the other area (Bowyer, 2016), demonstrating the population-level functional connectivity between the areas. Spike-field coherence, on the other hand, can be used to assess directional interaction, as spikes can be considered an output of a region, and LFPs correspond to an input into a region despite the fact that coherence itself is an non-directed method (Harvey et al., 2009; Okun et al., 2010; Stetson & Andersen, 2014; Vinck et al., 2012).

Another metric related to spike-field coherence is partial spike-field coherence. When there is a common driver for brain area A and B, with a larger effect on A compared to B, ordinary spike-field coherence would look like the spikes in A drive the activity in B, which is misleading because it doesn't account for C.

Partial spike-field coherence regresses out the effect of C, the common driver (Stetson & Andersen, 2014). The formula for calculating the partial spike-field coherence between spikes in area A and the field in area B is:

$$C_{S_A,A|B} = \frac{C_{S_A,B} - C_{S_A,A}\, C_{A,B}}{\sqrt{\left(1 - C_{S_A,A}^2\right)\left(1 - C_{A,B}^2\right)}},$$

where $C_{S_A,B}$ is the ordinary spike-field coherence between the spikes in area A (S_A) and the LFPs in area B, $C_{S_A,A}$ are another ordinary spike-field coherence between the spikes and LFPs in the same area A, and $C_{A,B}$ is the field-field coherence between LFPs in area A and B. By subtracting the interaction from spikes in A to the field in A, and then to the field in B, we can remove the effect of shared field oscillation between A and B and leave the selective interaction between spikes in A and the field in B (Stetson & Andersen, 2014). This metric can be useful when the power is asymmetric in the regions of interest, or if there is a larger-scale common driver.

2.4. Cortical plasticity

Plasticity, or the ability of the nervous system to respond to extrinsic and intrinsic factors by adopting a new functional or structural state (Ganguly & Poo, 2013), is crucial not only for the development of the nervous system, but also for normal brain function after development. It forms the biological basis for

learning and memory formation (Ganguly & Poo, 2013; Keller & Just, 2016), and it is also fundamental in the development and reorganization of neuronal circuits after neural injury (Nudo, 2014; Sanes & Donoghue, 2000).

Plasticity can take place in the macro, or anatomical, scale (Diamond et al., 1964; Hubel & Wiesel, 1998), as well as the micro, or cellular and subcellular, scale. Starting with Cajal's work, which suggested that changes in synaptic connections can serve as a substrate for memory (Cajal, 1913), there have been several studies on neural plasticity at the cellular level; for instance, Hebb postulated that correlated spikes between pre- and postsynaptic neurons may strengthen the connection between these neurons. Bliss and Lomo explored long-term potentiation (LTP) in the hippocampus (Bliss & Lomo, 1973), and Ito and Kano observed long-term depression (LTD) in the cerebellum (Ito & Kano, 1982). These discoveries led to further studies on plasticity, including spike-timing dependent plasticity (STDP), which demonstrated that precise timing of firing activity in pre- and postsynaptic neurons can induce LTP and LTD (Dan & Poo, 2004; Markram et al., 1997).

STDP strengthens the connection between two neurons when the presynaptic neuron fires before the postsynaptic neuron and weakens it when the presynaptic neuron fires after the postsynaptic neuron, which is consistent with Hebb's criterion on the correlation between spikes in pre- and postsynaptic neurons for strengthening the connections. This process has been shown both in in vitro studies (Bi & Poo, 2001; Caporale & Dan, 2008; Markram et al., 2011) and in

vivo studies with monkeys (Jackson et al., 2006; Nishimura et al., 2013). The in vivo studies involved an implantable electronic circuit to trigger electrical stimuli on one electrode by action potentials recorded on a different electrode, and successfully showed that such a device can artificially promote plasticity in the monkey brain based on STDP (Jackson et al., 2006; Nishimura et al., 2013). This finding shows that artificial connections in different brain sites established by closed-loop electrical stimulation can lead to plasticity changes in the actual neural connectivity between those sites, suggesting clinical applications in rehabilitation after neural injury.

2.5. Intracortical microstimulation for sensory feedback

The absence of somatosensory feedback in motor tasks substantially diminishes a person's performance (Sainburg et al., 1993), which greatly increases motivation in restoring sensation in neuroprosthetics. For an arm prosthesis, for example, it has been shown that a person's ability to control grasping strength can be significantly improved with artificial tactile feedback, enabling more dexterous manipulation of delicate objects (Tan et al., 2014). Recent work by us has demonstrated closed-loop circuits with BMIs, in which electrical intracortical microstimulation (ICMS) has become a promising tool for evoking somatosensory percepts in the primary somatosensory cortex (Armenta Salas et al., 2018; Klaes et al., 2014).

ICMS with different parameters can be detected and discriminated by non-human primates (NHPs) (Dadarlat et al., 2015; Romo et al., 1998, 2000; Tabot et al., 2013), and can be incorporated as sensory feedback in BMI tasks (Klaes et al., 2014; O'Doherty et al., 2011). Furthermore, in recent human studies, a wide range of sensations elicited from ICMS has been reported (Armenta Salas et al., 2018; Flesher et al., 2016). There are, however, more stimulation parameters that have not been explored in human studies yet. Flesher et al. focused on the effect of stimulation amplitude (Flesher et al., 2016), and in our previous research, we changed stimulation amplitude and frequency to evoke different sensations (Armenta Salas et al., 2018); other parameters, such as pulse width and pulse train duration, may affect stimulation thresholds and/or elicited percepts, as suggested in monkey work (Kim et al., 2015). Exploring such a large parameter space requires substantial amounts of time given the manual processes involved in configuring each stimulus and receiving verbal feedback about each percept.

Another challenge associated with artificially evoking somatosensory percepts is the expected need for frequent recalibration. Sensory streams are continuously recalibrating to provide statistically efficient feedback (Burge et al., 2010; Dadarlat et al., 2015; Ernst & Banks, 2002; Gu et al., 2008; McGuire & Sabes, 2009; Simani et al., 2007; Sober & Sabes, 2005; van Beers et al., 1999; Verstynen & Sabes, 2011). Therefore, as in cortical visual prosthetics (Dowling, 2005) or stimulation in auditory cortex (Koivuniemi & Otto, 2012), ICMS for somatosensory feedback would also require frequent recalibration—perhaps

daily. Calibration is a tedious and time-consuming process in which the experimenter must test each parameter on each electrode to establish thresholds and outcomes.

Chapter 3

CHARACTERIZATION OF NEURAL CONNECTIVITY

3.1. Introduction

Previous work in monkeys and humans has shown that the supramarginal gyrus (SMG), ventral premotor cortex (PMv), anterior intraparietal (AIP), and Brodmann's area 5 (BA5) play distinct roles during movement planning and execution, suggesting possible neural connections between them. SMG, AIP, and PMv in the left hemisphere, for example, have been associated with control of hand-object interactions (Andres et al., 2017; Brandi et al., 2014; Johnson-Frey et al., 2005; Kroliczak & Frey, 2009). Neurons in PMv are known to be responsive to tactile stimuli (Fogassi et al., 1996), and SMG is responsible for integrating tools into the body schema (Fabbri et al., 2016; Rozzi et al., 2008). Neural activity in AIP and BA5 codes for grasp planning and arm movements (Aflalo et al., 2015; Klaes et al., 2015).

However, relatively little is known about the exact interface governing connections between these areas, and how they interact during certain behaviors. Stetson and Andersen have shown that the spike activity in the parietal reach region (PRR) of monkey anti-synchronizes with LFP in the dorsal premotor cortex (PMd) relative to global beta-band activity, which diminishes connectivity despite high field coherence and spike-field coherence between them (Stetson & Andersen, 2014). This finding suggests that, even though the aforementioned

brain areas are strongly active during certain tasks, their spikes might be anti-synchronized with LFP in other areas, diminishing communication rather than enhancing it.

In this study, therefore, connectivity between AIP and BA5, and between SMG and PMv in human subjects was characterized in more detail, based on field-field coherence, spike-field coherence, and partial spike-field coherence. With different types of behavioral tasks, such as imagining or executing movements, receiving tactile stimuli, and counting numbers, we show that imagined/executed movements and tactile stimuli induce a decrease in LFP power in all the regions and normal/partial spike-field coherence in all the pairs of the regions, whereas counting numbers does not. We further demonstrate that the phase in partial spike-field coherence can reveal the selective interaction between PMv and SMG, which suggests that spikes in PMv may enhance the communication with SMG. This will also help us understand the communication in parietal area, and establish a baseline neural connectivity for exploring how stimulation affects these patterns of activity.

3.2. Methods

3.2.1. Subject

Two tetraplegic patients have participated in the study. Subject EGS was a male tetraplegic patient, who was 32 years old, 10 years post-lesion at the time of implantation. He had a complete C3/C4 spinal cord injury, which led to paralysis of all limbs. Subject FG, on the other hand, was a 32-year-old male tetraplegic patient who was 1.5 years post-injury at the point of recruitment for a clinical trial of a BMI system with intracortical recording and stimulation. He suffered a complete C5/C6 spinal cord injury, but has some residual sensation in his upper arm (anterior-radial section and posterior-radial section) and forearm. All experimental procedures for both patients were reviewed and approved by the Institutional Review Boards (IRB) of the University of Southern California (USC) and Rancho Los Amigos National Rehabilitation Hospital (RLA). The implantation of the electrodes was done at Keck Hospital of USC, and the study sessions were held at RLA for EGS, and RLA and the patient's house for FG.

3.2.2. Experimental setup

All the tasks were performed while the subjects were seated in their wheel chair (at RLA) or on their bed (at the patient's house). The tasks were

displayed on a 27-inch LCD monitor in a lit room using Psychophysics Toolbox (Brainard, 1997) for MATLAB.

3.2.3. Experimental design

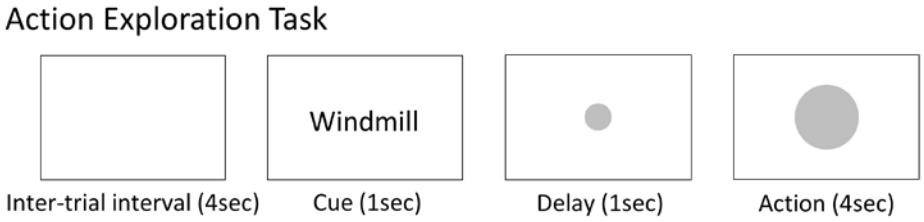

Figure 3.1. Design of action exploration task. The subject has to imagine or execute cued action during action phase for four seconds. Two different groups of action classes was used: one with imagining grasping, scratching, rotating the arm, and counting, and the other with actually moving the arm and being touched on the neck.

To characterize the connectivity between different brain areas, we ran a behavioral task called action exploration task, with two different sets of actions (Figure 3.1). In one version, we cued one of four behaviors—open and closed grip (for grasping), scratching the back of the head, windmill (rotating the arm), and counting (counting numbers in one's head)—and the subject imagined performing cued behaviors during an action phase. As this task employs not only motor imagery of arm and hand movements (grasping, scratching, and rotating the arm) but also a mental process that does not include any motor action (counting), the activity of the brain regions of interest and their interactions can be compared between those groups. The

other version of the task, which was done only with FG, included some volitional physical movement and tactile stimuli; in this version, depending on the cue shown in each trial, the subject moved his arm (depending on the presence of residual movement), or the experimenter touched the subject's neck with three light downward strokes.

3.2.4. Signal recording

Subject EGS was implanted with two 96-channel, platinum-tipped Neuroport microelectrode recording arrays (Blackrock Microsystems, Salt Lake City, UT) in AIP and BA5. The microelectrodes in each of the arrays were 1.5 mm long, and were arranged in a 10-by-10 grid with 400-μm space. Preoperative fMRI tasks following the protocols described in our previous study (Aflalo et al., 2015) were used for surgical planning.

Subject FG was implanted with the same Neuroport arrays in SMG and PMv, with additional two 7-by-7 sputtered iridium oxide film (SIROF)-tipped microelectrode arrays in S1. Preoperative fMRI tasks based on our previous experiment (Aflalo et al., 2015) were also used to identify these brain areas for surgical planning, with additional tasks described in (Armenta Salas et al., 2018) to identify the location of S1.

3.2.5. Statistics and analysis methods

To examine the population-level activity in each brain area during different mental and behavioral tasks, we computed the power spectra in overlapping windows of 0.5 seconds, with step size of 0.25 seconds, from each channel in each session. The raw power spectrum from each session was then normalized based on the LFP power during the last one second of the inter-trial interval, and the resulting z-scores were used to get the population-averaged spectrogram during each mental and behavioral task.

To investigate the neural connectivity during the task, field-field, spike-field, and partial spike-field coherence was calculated in overlapping windows of 0.4 s, with step size 0.2 s, using the multi-taper method with 5 tapers and time-bandwidth parameter of 3 (Bokil et al., 2010). All sessions were integrated into the coherence analysis by averaging the spectrum and cross spectrum across all of the sessions, rather than averaging the final coherence values from each session. For spike-field coherence and partial spike-field coherence, we used the channels with firing rates over 0.1 Hz in all of the sessions for both the spike and LFP measurement, to take only stable channels into the calculation. The resulting coherence values were all z-scored based on previous research (Jarvis & Mitra, 2001), to easily visualize the statistical significance.

For the LFP power and coherence in the frequency range of interest, temporal patterns during each of the mental and behavioral tasks were compared using Kolmogorov-Smirnov test. A t-test was used to compare the difference between the means of the distributions of these values in each phase of the trial in each task.

3.3. Results

3.3.1. LFP power during motor imagery

In order to explore the activity in the recording area during mental imagery, LFP power spectrum was investigated. We found that LFP power in the beta frequency range (12-30Hz) decreases during mental imagery of motor movement in SMG, PMV, AIP, and BA5, although how long the decreased coherence is maintained varied across different arrays and different actions (Figure 3.2B–3.2E). This result is consistent with previous research about sensorimotor rhythm and event-related desynchronization (Leocani et al., 2001); however, the increase in the LFP power during the planning phase shown in a previous study (Stetson & Andersen, 2014) was not found. In our experiment, such a preparatory signal was found during the cue phase, but it was only a slight increase.

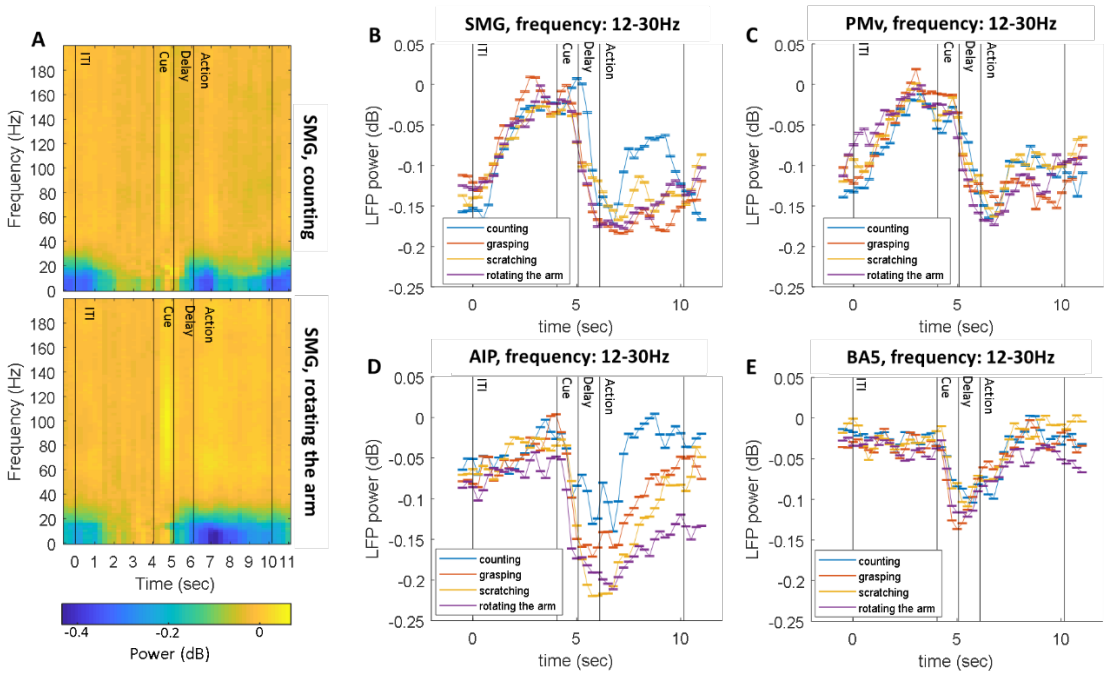

Figure 3.2. LFP power spectrum during mental imagery. Example power spectrum during counting numbers (top) and imagined grasping (bottom), measured in SMG. B–E) Changes in LFP power in beta frequency range (12–30Hz) during different imagery, measured in SMG (B), PMv (C), AIP (D), and BA5 (E).

Another notable thing is that counting, which does not entail any motor imagery, shows less of a decrease in beta power during action phase, especially in SMG and AIP. It still shows a decrease at the action onset, but it increases back to the baseline much faster than any other motor imagery. In SMG and AIP, changes in LFP power during the action phase with counting were significantly different from the changes during any other motor imagery (Kolmogorov–Smirnov test; $p<0.005$ for SMG, and $p<0.0001$ for AIP). This is also consistent with previous studies relating event-related

desynchronization in the beta band with motor output and imagery (Leocani et al., 2001; Pfurtscheller et al., 2005; Ranade et al., 2009).

3.3.2. Field-field coherence during motor imagery

In field-field coherence, as with LFP power, we found a peak for both motor imagery and mental process without any imagined movement (counting) in the beta band in both SMG-PMv and AIP-BA5 (Figure 3.3A, S5, S6). The difference between motor imagery and counting, however, was not as evident as it was for the LFP power shown above. Field-field coherence in AIP-BA5 was clearer than in SMG-PMv, both in terms of the magnitude and the difference between motor imagery and counting, but the changes in coherence during counting significantly differed only from the motor imagery of scratching the back of the head (Kolmogorov–Smirnov test; $p<0.001$). Increase in the field-field coherence during planning, which was found in a previous study (Stetson & Andersen, 2014), has also not been found.

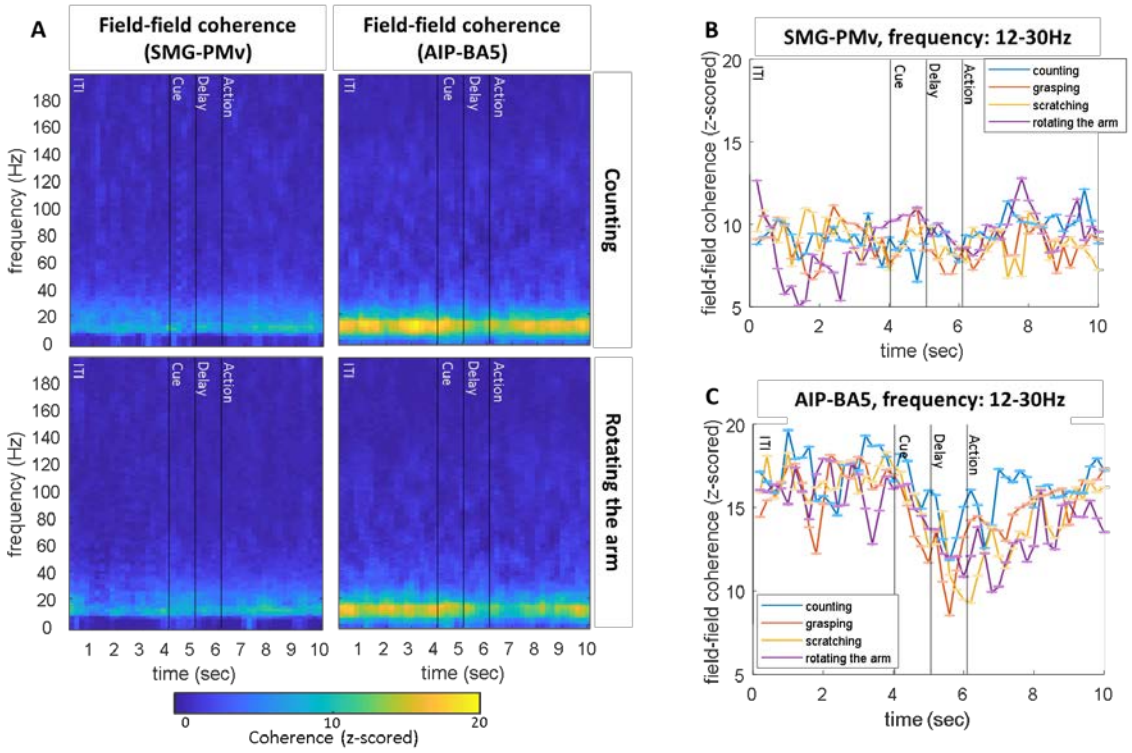

Figure 3.3. Field-field coherence during mental imagery. A) Example field-field coherence during counting (top) and rotating the arm (bottom), measured between SMG and PMv (left), and between AIP and BA5 (right). For both counting and rotating the arm, the peak coherence was observed at 15.6 Hz between SMG and PMv, and 13.7 Hz between AIP and BA5. B-C) Field-field coherence in beta frequency range (12-30Hz) between SMG and PMv (B), and between AIP and BA5 (C), during different mental imageries.

3.3.3. Spike-field coherence during motor imagery

We found a peak in spike-field coherence in the alpha band between SMG and PMv, both with SMG spikes and PMv fields, and with PMv spikes and SMG fields (Figure 3.4). It was at 11.7 Hz, which is in the alpha band (8–12Hz), rather than the beta band shown in previous results with LFP power and field-field coherence. It also showed a decrease during the action phase

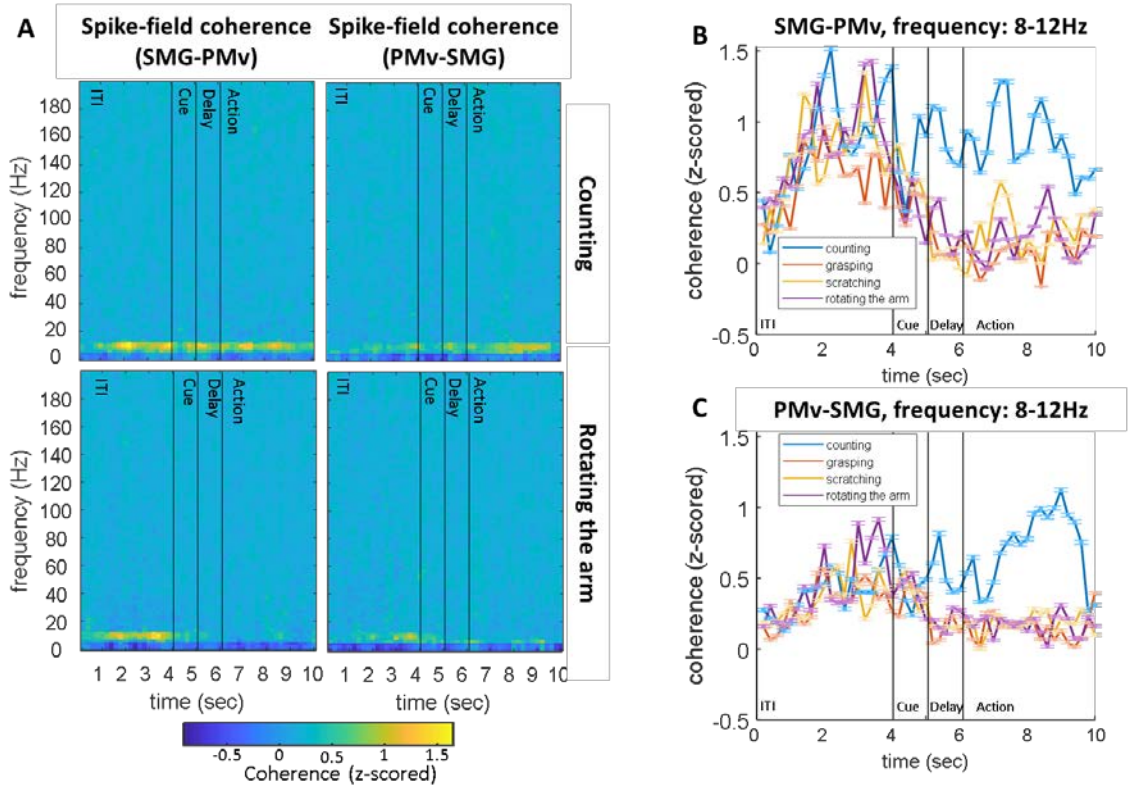

Figure 3.4. Spike-field coherence during mental imagery. A) Example spike-field coherence during counting (top) and rotating the arm (bottom), measured between spikes in SMG and LFP in PMv (left), and between spikes in PMv and LFP in SMG (right). During counting numbers and ITI, the peak coherence was observed at 11.7 Hz in both SMG-PMv, and PMv-SMG spike-field coherence. B-C) Spike-field coherence in alpha frequency range (8–12 Hz) between spikes in SMG and LFP in PMv (B), and between spikes in PMv and LFP in SMG (C), during different mental imageries.

with motor imagery; however, for counting, the decrease was not as significant as during motor imagery. For the coherence between spikes in PMv and fields in SMG, it even increased during the action phase (Figure 3.4C). In the Kolmogorov-Smirnov test, the spike-field coherence between SMG and PMv during counting numbers were significantly different from that during any other motor imagery ($p<10^{-6}$) both directions—spikes from

SMG and LFP from PMv, and vice versa—whereas all the other combinations of imagery did not return any significant p-values. We also examined the spike-field coherence between AIP and BA5, but no significant changes were found, possibly due to low firing rate from the units.

3.3.4. Partial spike-field coherence during motor imagery

We also found a similar pattern in partial spike-field coherence in the alpha band between SMG and PMv (Figure 3.5). The peak coherence was found at 11.7 Hz, as in the normal spike-field coherence. Other patterns, including the decrease during motor imagery, and the increase during counting—especially for spikes in PMv and LFP in SMG—were also the same as in the normal spike-field coherence. The partial spike-field coherence between SMG and PMv during counting numbers was significantly different from that during motor imagery ($p<10^{-5}$; Kolmogorov–Smirnov test) in both directions; between different types of motor imagery, however, the partial spike-field coherence was not significantly different. The partial spike-field coherence between AIP and BA5 was not investigated since the normal spike-field coherence did not show any significant values.

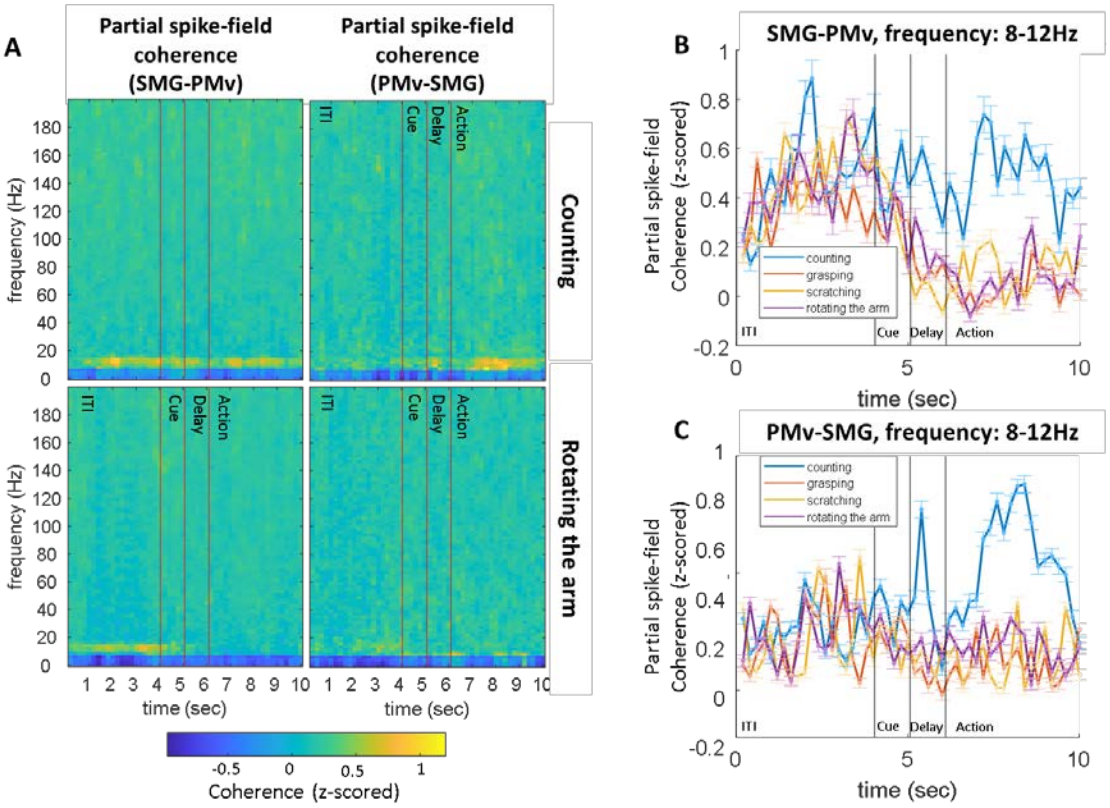

Figure 3.5. Partial spike-field coherence during mental imagery. A) Example of partial spike-field coherence during counting (top) and rotating the arm (bottom), measured between spikes in SMG and LFP in PMv (left), and between spikes in PMv and LFP in SMG (right). During counting numbers and ITI, the peak coherence was observed at 11.7 Hz in both SMG-PMv, and PMv-SMG partial spike-field coherence. B-C) Partial spike-field coherence in alpha frequency range (8–12 Hz) between spikes in SMG and LFP in PMv (B), and between spikes in PMv and LFP in SMG (C), during different mental imageries.

Although general patterns in the magnitudes of coherence are similar between spike-field coherence and partial spike-field coherence, the phase of the coherence shows differences. Figure 3.6 shows the phase of spike-field coherence and partial spike-field coherence between spikes in PMv and LFP in SMG during counting numbers. Even though the phase in normal spike-field coherence is around 300–330 degrees, the partial spike-field coherence

reveals that the spike in PMv is actually phase-locked with the peak of the LFP in SMG if we remove the effect of the common driver, showing that PMv might drive the activity in SMG.

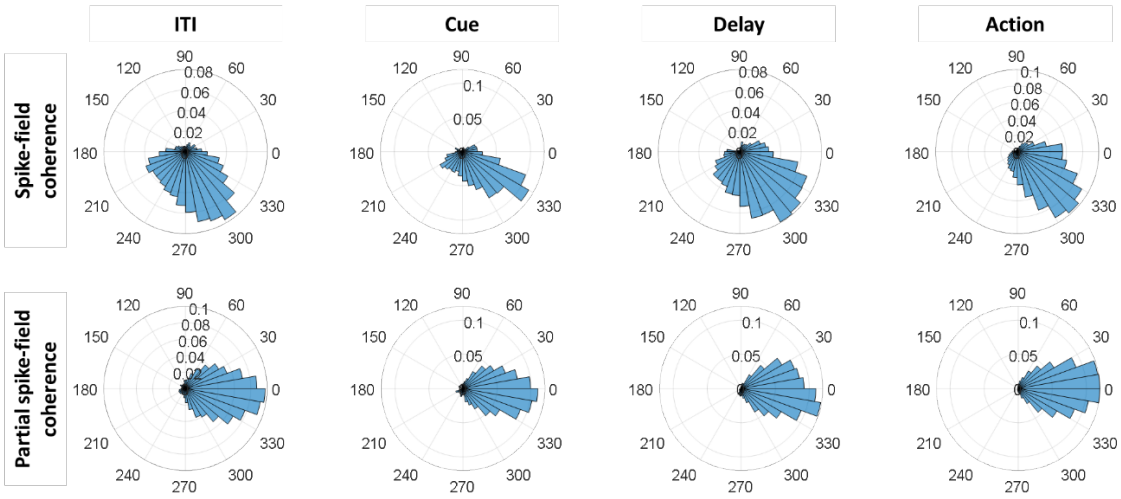

Figure 3.6. Comparison of phase distributions: Phase of spike-field coherence (top) and partial spike-field coherence (bottom) with spikes from PMv and LFPs in SMG, for the action exploration task of counting numbers. Partial spike-field coherence reveals that the spikes in PMv are locked well with the LFPs in SMG with a phase of 0, even though it was not clear in spike-field coherence.

3.3.5. LFP power during actual movement and tactile stimuli

We found a pattern of LFP power during the action exploration task with actual arm movement and tactile stimuli on the neck that is similar to what we saw during the same task with motor imagery and counting numbers; the power in the low-frequency range, namely the beta band, decreased during cue, delay, and action, and increased back at the end of return phase (Figure 7). However, there was an increase in power after the onset of cue phase for

tactile stimuli, and another slight increase in the beginning of delay phase for moving up the arm (Figure 7B-C), which may be a sign of the preparatory signal shown in a previous study (Stetson & Andersen, 2014). Furthermore, the power decrease during tactile stimuli was larger than that during motor movements, which is in contrast with previous studies associating event-related desynchronization in the beta band with motor output and imagery (Leocani et al., 2001; Pfurtscheller et al., 2005; Ranade et al., 2009).

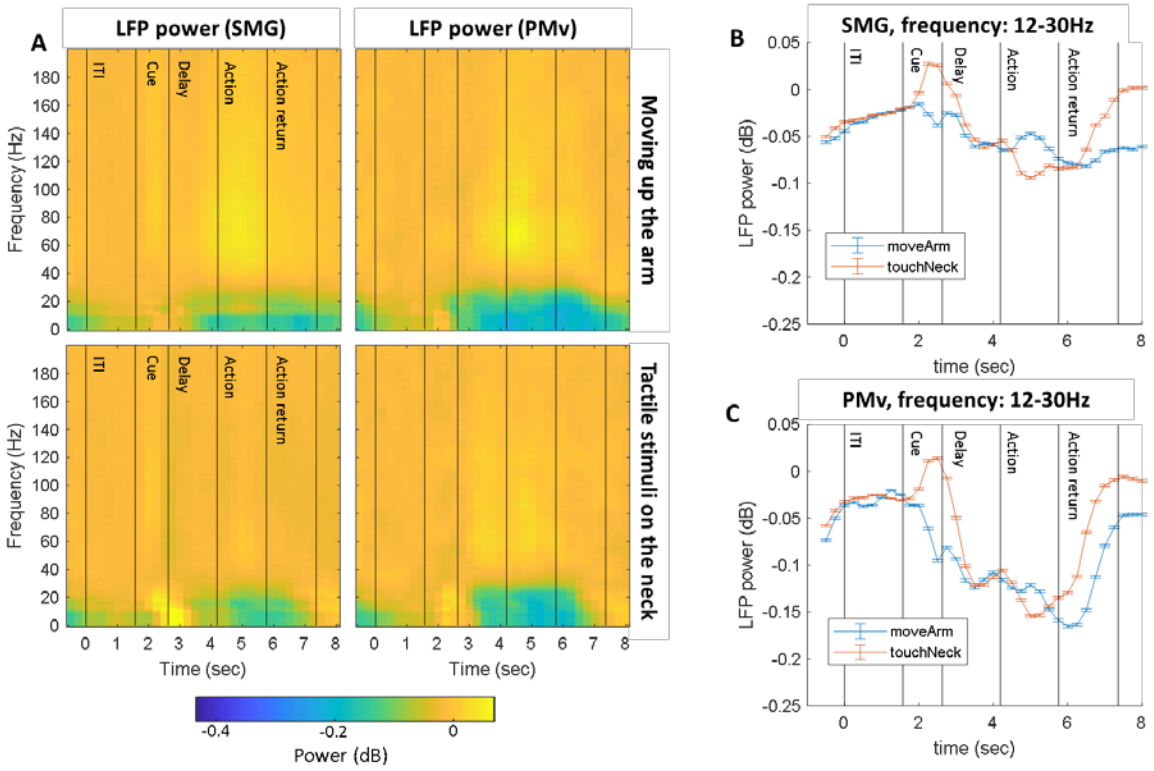

Figure 3.7. LFP power from SMG and PMv during the action exploration task with arm movements and tactile stimuli on the neck. A) Example of population-averaged spectrogram during moving up the arm (top) and tactile stimuli on the neck (bottom), measured from SMG (left), and in PMv (right). B-C) LFP power in the beta frequency range (12-30 Hz) in SMG (B), and in PMv (C), during different sensory/motor tasks.

3.3.6. Field-field coherence during actual movement and tactile stimuli

Field-field coherence between SMG and PMv during arm movement and tactile stimuli also showed a significant peak activity in the beta band (12–30Hz), similar to field-field coherence between SMG-PMv and AIP-BA5 during action exploration task with motor imagery and counting numbers (Figure 3.3). One important difference, however, was that with actual arm movements and tactile sensations, we could find an increase in field-field coherence during delay that decreases back during the action phase, which we could not find with motor imagery. The increase in the field-field coherence was more prominent during arm movement, as shown in Figure 3.8B. This suggests that the reason we could not find significant a preparatory signal as in previous studies (Stetson & Andersen, 2014) during

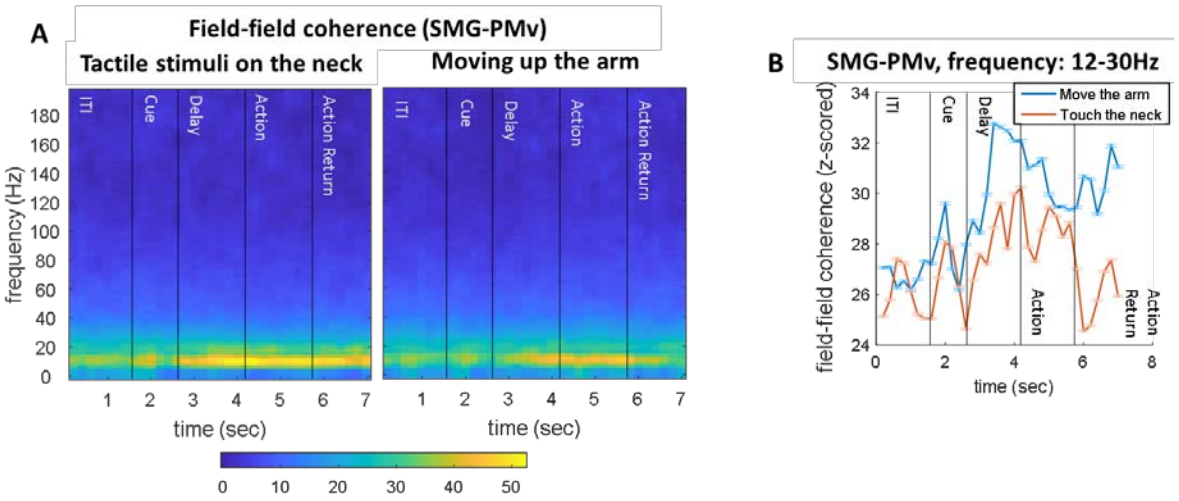

Figure 3.8. Field-field coherence between SMG and PMv during action exploration task with arm movement and tactile stimuli on the neck. A) Population-averaged coherogram during tactile stimuli on the neck (left), and moving up the arm (right). B) Temporal changes in average coherence in 12–30Hz (population averaged). Every coherence value shown here is normalized.

action exploration was maybe because we used motor imagery, not an actual movement.

3.3.7. Spike-field coherence and partial spike-field coherence during actual movement and tactile stimuli

In spike-field coherence and partial spike-field coherence, we also found a peak in the alpha band (Figure 3.9A, 3.10A). It was more prominent for spikes in PMv and LFP in SMG, rather than spikes in SMG and LFP in PMv. The temporal changes in coherence over the course of the task were similar to those with motor imagery: the coherence goes down during the cue phase and comes back up at the end of the action or action return phase, with one exception of the SMG to PMv partial spike-field coherence during moving the arm, where the coherence increases during the action phase (Figure 3.9B-3.9C, 3.10B-3.10C). As mentioned earlier in the field-field coherence, this contrasts with the previous study on coherence during motor imagery and motor outputs.

We also investigated the phase of coherence in normal spike-field coherence and partial spike-field coherence. Figure 3.11 shows the phase of such coherences measured between spikes in PMv and LFPs in SMG. As shown in the first and third row, the phase of spike-field coherence is unstable—the figure shows a lot of different phases, instead of showing a single

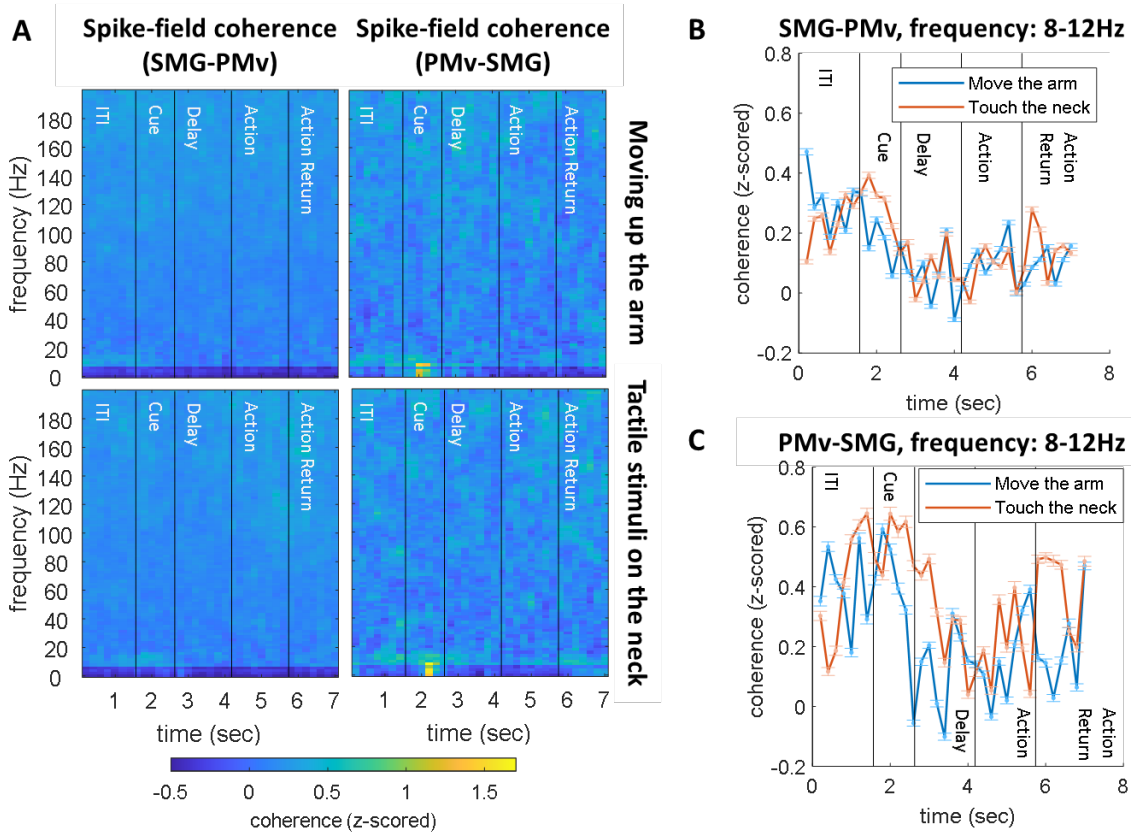

Figure 3.9. Spike-field coherence during motor output and sensory input. A) Example spike-field coherence during moving up the arm (top) and tactile stimuli on the neck (bottom), measured between spikes in SMG and LFP in PMv (left), and between spikes in PMv and LFP in SMG (right). During cue phase, the peak coherence was observed at 9.8 Hz in PMv-SMG spike-field coherence. B-C) Spike-field coherence in alpha frequency range (8–12 Hz) between spikes in SMG and LFP in PMv (B), and between spikes in PMv and LFP in SMG (C), during different sensory/motor tasks.

distribution centered at a certain point. However, the phase of the partial spike-field coherence is much cleaner, and it is centered at the phase of zero, which demonstrates the possible excitatory effect that the spikes from PMv

have on SMG. We also explored the phase of coherence between spikes in SMG and LFPs in PMv, but a significant pattern was not found.

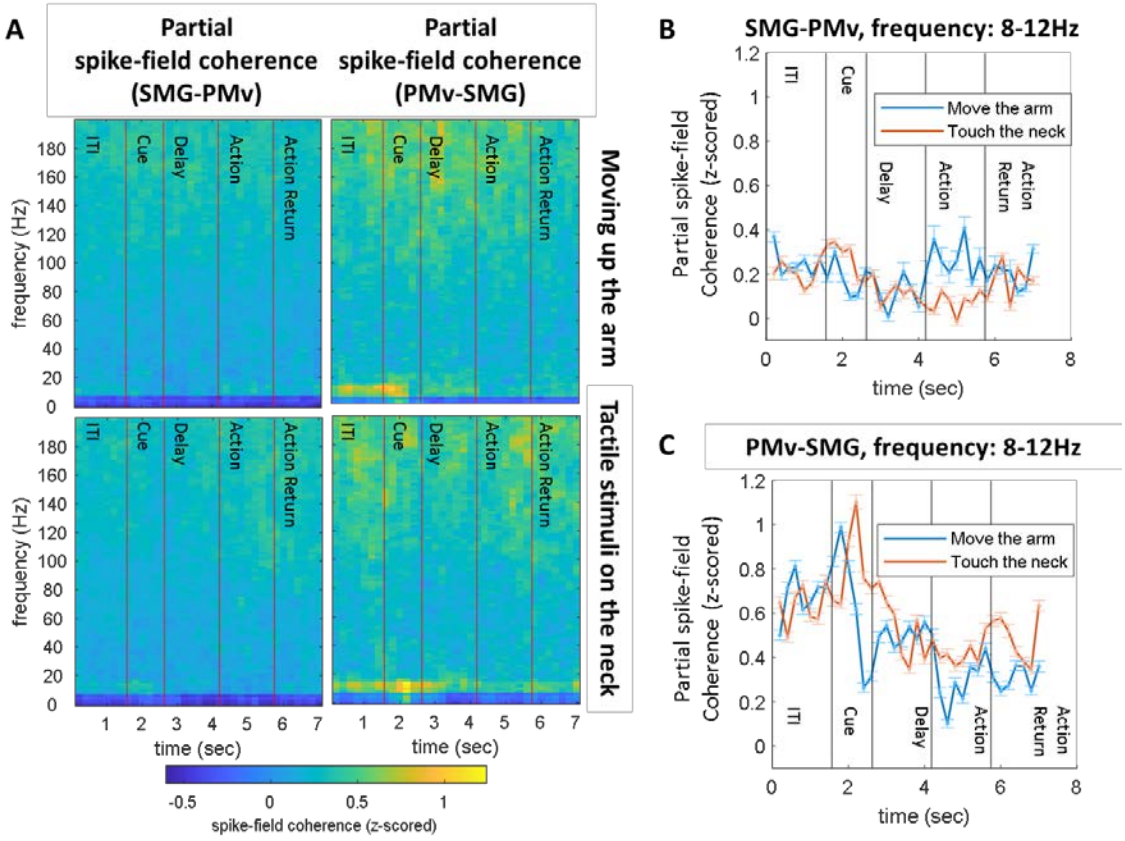

Figure 3.10. Partial spike-field coherence during motor output and sensory input. A) Example partial spike-field coherence during moving up the arm (top) and tactile stimuli on the neck (bottom), measured between spikes in SMG and LFP in PMv (left), and between spikes in PMv and LFP in SMG (right). During ITI and cue phase, the peak coherence was observed at 9.8 Hz in PMv-SMG spike-field coherence. B-C) Partial spike-field coherence in alpha frequency range (8-12 Hz) between spikes in SMG and LFP in PMv (B), and between spikes in PMv and LFP in SMG (C), during different sensory/motor tasks.

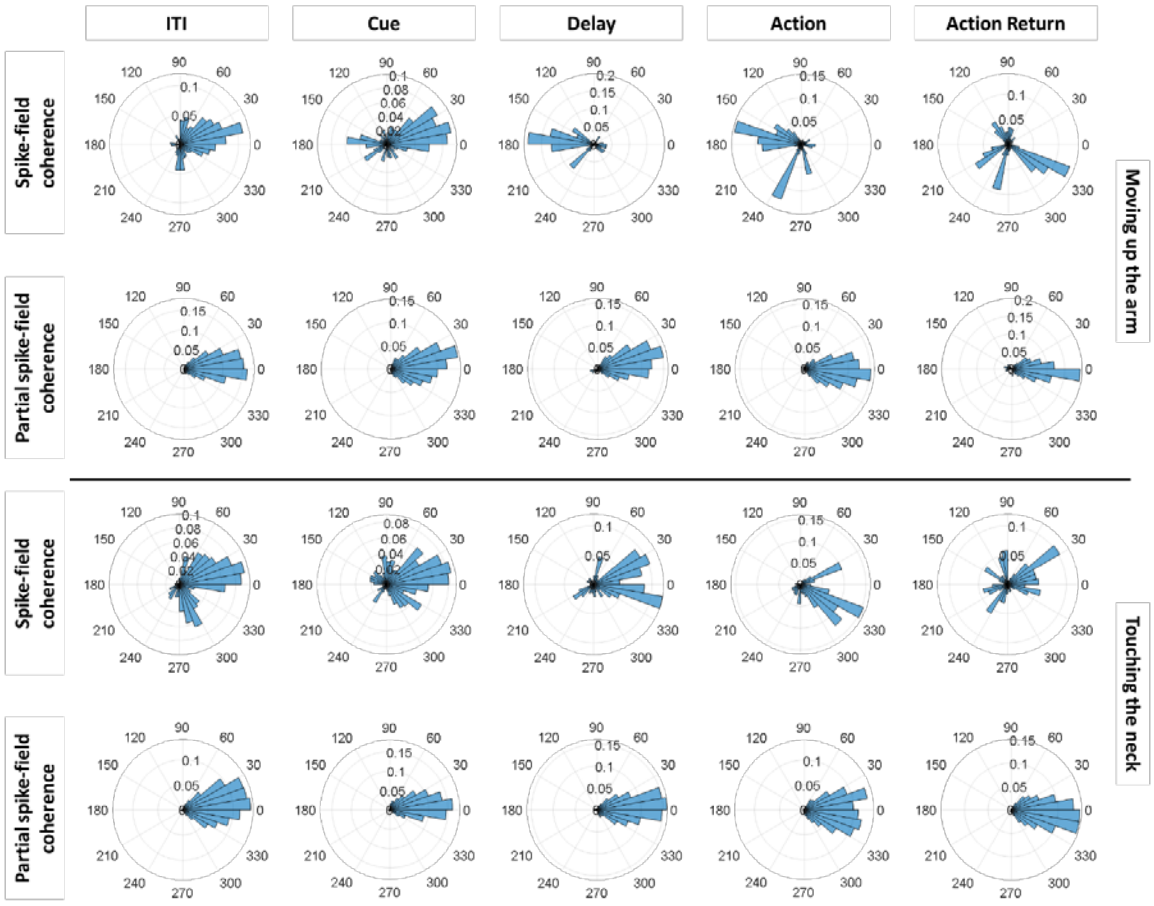

Figure 3.11. Comparison of phase distributions: Phase distribution of spike-field coherence and partial spike field coherence during the “moving the arm” trial (top) and “touching the neck” trial (bottom), between spikes in PMv and LFPs in SMG. Each column corresponds to each phase of the trial.

3.4. Discussion

In this study, we explored LFP power and field-field, spike-field, and partial spike-field coherence measured in the parietal area during different tasks. For LFP power, we have found a decrease in the beta band during motor imagery and

motor output, which is consistent with the previous research on SMR (Pfurtscheller et al., 2005; Pfurtscheller & Lopes da Silva, 1999; Pfurtscheller & Neuper, 1997). Counting numbers, which does not entail any motor component, also showed a decrease in LFP power in the beta band, but it was much more transient than during the motor imagery and motor outputs. However, an increase in the LFP power during planning of the movement, which was evident in the previous research (Stetson & Andersen, 2014), was not found during either the cue and delay phases in our study. There was a slight increase in the power during the cue phase for motor imagery and motor output, but it was not as big as previously reported. This might be due to the different types of task. For the motor outputs, our task focuses only on the motor planning with a single effector and single target, whereas Stetson's paper included decision-making processes for the choice of different types of effector (saccade vs. reaching). For the motor imagery, on the other hand, it lacks the actual motor output that exists in the tasks with eye and hand movements. Such different processes and outputs involved in the task might have led to different LFP patterns during the planning phase. Further investigation with a new task involving a decision-making component similar to the one in Stetson's paper would be necessary to investigate the preparatory signal.

An interesting pattern we found in LFP power is that there is an increase in beta power during the cue phase for tactile stimuli on the neck. One may argue that the visual cue shown on the screen during the cue phase might have caused such

an increase in the LFP power; however, the same type of cues was also used in the trials with motor imagery and motor output, and they did not show significant increase in LFP power during the cue phase. Therefore, this cannot explain the pattern we found only in the cue for tactile stimuli. One possible explanation would be an expectation for the tactile stimuli. According to a previous study with magnetoencephalography recording, it has been shown that the beta oscillations in the parietal cortex are positively correlated with the states of anticipation and with the tactile detection performance (Buchholz et al., 2014; Linkenkaer-Hansen et al., 2004; van Ede et al., 2010). As the subject in our study also would have anticipated the tactile stimuli on the neck given the cue, the increased beta power during the cue phase might be from such anticipatory activity.

For field-field coherence, high coherence was observed also in the beta band for both SMG-PMv and AIP-BA5, but the decrease during imagined movements was only observed in AIP-BA5. SMG-PMv exhibited a decreased field-field coherence only during executed movements, although it was still higher than the baseline in ITI, but not during the imagined action or tactile stimuli. Interestingly, it also showed a significant increase during the delay phase for moving the arm— but not during the motor imagery—which is consistent with the previous study (Stetson & Andersen, 2014). Such differences between motor output and motor imagery reflect that the beta band in the parietal area may have

some role in suppressing possible movements, as suggested in previous research (Stetson & Andersen, 2014).

Spike-field coherence and partial spike-field coherence shared a similar pattern of gradually decreasing coherence from the cue phase to the action phase during imagined movements and tactile stimuli. Executed movements also showed similar patterns except for the partial spike-field coherence between SMG and PMv, where the coherence was slightly increased during the action phase. Counting numbers, in contrast, showed an increased coherence from delay phase to action phase. The decrease in spike-field coherence during the planning period (cue and delay phase) before motor imagination or execution is inconsistent with the previous study (Stetson & Andersen, 2014), which might be due to the different structure of the tasks as mentioned above. Lack of fine control of the arm is another possible reason, since the participant did not have full control of the arm—only weak residual control of the biceps.

One interesting pattern we found in the normal and partial spike-field coherence was that the phases of partial spike-field coherence between spikes in PMv and fields in SMG during counting, motor output and sensory input were tightly distributed around 0, whereas the phase in spike-field coherence was not; it was unstable in the trial with motor outputs and sensory inputs (Figure 3.11), and during counting it was around 300–330 degrees. This shows how partial spike-field coherence can reveal the actual connectivity between spikes and LFPs, after removing the effect of common driver. Although the spike-field coherence

between PMv and SMG during motor execution and tactile stimuli looks as if there are no clear patterns shared in the connections from PMv to SMG, the partial spike-field coherence suggests that PMv might actually drive the activity in SMG, since its phase is zero. The partial spike-field coherence during counting numbers also suggests the same relationship between PMv and SMG, although it was not clear in spike-field coherence.

Our study shows a different pattern of activity and connectivity during different behavioral tasks. It also reveals the directional interaction from PMv to SMG through partial spike-field coherence, which was obscured in spike-field coherence. This helps us understand the network in the parietal cortex and provides a baseline connectivity that can be used to identify changes in functional connections after stimulation, which would be important to study the effect of neural stimulations.

Chapter 4

PROMOTION OF CORTICAL PLASTICITY THROUGH SPIKE-TRIGGERED STIMULATION

4.1. Introduction

Artificial plasticity promotion has been shown previously in various in vivo experiments in animal studies. For example, spike-triggered stimulation of one brain site, triggered from spikes or beta oscillations recorded in another site, can modify synaptic connections between the sites in monkeys (Jackson et al., 2006; Nishimura et al., 2013; Zanos et al., 2018). However, this paradigm has not yet been established in humans. In this study, we present novel findings on how measures of neural connectivity in the human brain can change in the presence of electrical stimulation. By delivering spike-triggered stimulation to channels with a preexisting connectivity pattern, identified based on coherence, we found the spike time tiling coefficient (STTC) between areas can be significantly increased in a subset of channel pairs. Our results also show that the connectivity within the stimulated area can be both strengthened and weakened, depending on different channel pairs after any type of stimulation, whether it is spike-triggered or random. This demonstrates the ability to artificially modulate plasticity using bidirectional BMIs in humans, which can be beneficial in rehabilitation after neurological diseases.

4.2. Methods

4.2.1. Subject

Subject FG was a 32-year-old male tetraplegic patient who was 1.5 years post-injury at the point of recruitment for a clinical trial of a BMI system with intracortical recording and stimulation. He suffered a complete C5/C6 spinal cord injury, but has some residual sensation in his upper arm (anterior-radial section and posterior-radial section) and forearm. All experimental procedures were reviewed and approved by the Institutional Review Boards (IRB) of the University of Southern California (USC) and Rancho Los Amigos National Rehabilitation Hospital (RLA). The implantation of the electrodes was done at Keck Hospital of USC, and the study sessions were held at RLA and the patient's house.

4.2.2. Experimental setup

All the tasks were performed while the subject was seated in his wheel chair (at RLA) or on his bed (at the patient's house). The tasks were displayed on a 27-inch LCD monitor in a lit room using Psychophysics Toolbox (Brainard, 1997) for MATLAB.

4.2.3. Experimental design

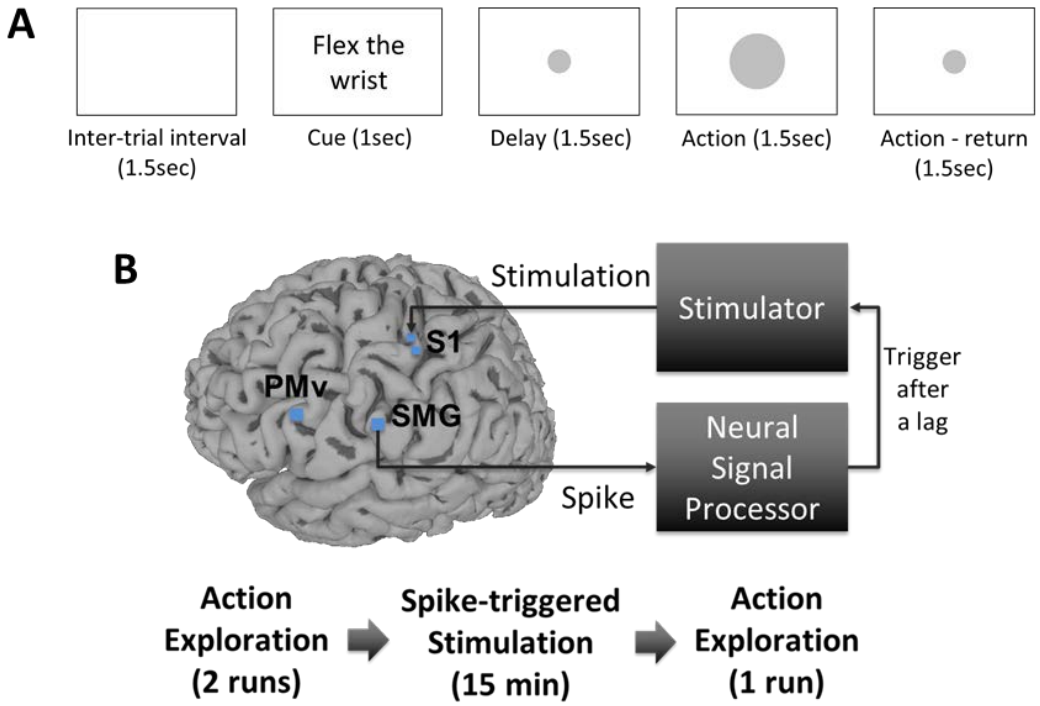

Figure 4.1. Experimental design for quantifying functional neural connectivity and its changes after stimulation. A) The design of the action exploration task. During the action phase, the subject was asked to execute or imagine the action shown in the cue phase, and the neural signals measured while doing so were used to quantify neural connectivity. B) The overall task design. It starts with two runs of aforementioned action exploration task to measure the baseline connectivity, which was followed by spike-triggered stimulation for 15 minutes, and another action exploration task to assess the changes in the neural connectivity. During the spike-triggered stimulation task, measured spikes from the selected channel in SMG triggered stimulation in S1.

To measure the neural connectivity during different activities, such as imagining or executing motor outputs and passively receiving tactile stimuli, we ran an action exploration task (Figure 4.1A). In this task, we showed a short phrase describing an action, and then asked the subject to do or

imagine the given action, with an exception of receiving tactile stimuli where the subject passively got the tactile stimuli from the experimenter. We ran five different types of action exploration task with different action classes: imagined arm movements, imagined finger movements, imagined reach, tactile stimuli, and imagined/executed movements which shared a few action classes used in imagined arm movements. The neural activity during the given action (action phase in Figure 4.1A) was used in a neural connectivity analysis, and two action classes, lifting up the arm and receiving tactile stimuli on the neck, which yielded the highest field-field coherence, were used in the following experiments.

To assess the effect of the closed-loop stimulation on neural connectivity, we designed a spike-triggered stimulation task and combined it with the aforementioned action exploration tasks before and after the stimulation (Figure 4.1A). The action exploration task used the selected action classes mentioned above: lifting up the arm or receiving tactile stimuli on the neck (three downward strokes). The first two runs of such a task (pre-stim) were used to quantify the baseline neural connectivity, and the one that ran after the stimulation (post-stim) was used to identify the changes in connectivity after stimulation.

For the spike-triggered stimulation task (10 sessions), we stimulated S1 at a fixed lag (20 ms) from threshold crossings recorded in SMG of the subject for 15 minutes. For stimulation, we delivered a single, biphasic, charge-

balanced cathodic pulse with an amplitude of 50 μA. The pulse width was 200 μs, and the interphase interval was 53 μs. In a closed-loop condition, with the patient at rest, stimulation was delivered over 15 minutes to eight channels in S1, selected to include the electrode with the highest partial spike-field coherence with SMG in the pre-stim task, and spacing the remaining seven to limit charge per phase per area. During this task, the subject repeatedly raised his arm according to the cue shown on the screen at random points, to activate the same neural connections that were used during the pre-stim action exploration task.

For the control condition, we used two different settings: random stimulation (four sessions), and no stimulation (three sessions). For the random stimulation control, two channels in S1 were randomly selected, and the stimulation pulses were delivered at random points with an average rate equal to that of the stimulation condition mentioned above. For the no stimulation condition, on the other hand, stimulation pulses were not delivered at all. For both of these conditions, the settings other than the stimulation parameters remained the same, including the behavioral task.

4.2.4. Signal recording

Subject FG was implanted with two 96-channel, platinum-tipped Neuroport microelectrode recording arrays (Blackrock Microsystems, Salt Lake City,

UT) in SMG and PMv, with additional two 7-by-7 sputtered iridium oxide film (SIROF)-tipped microelectrode arrays in S1. The impedance of SIROF-tipped electrodes is lower than that of platinum-tipped electrodes, which makes it more suitable for stimulation. Preoperative fMRI tasks based on (Aflalo et al., 2015) were used to identify these target brain areas for surgical planning, with additional tasks described in (Armenta Salas et al., 2018) to identify the location of S1.

4.2.5. Statistics and analysis methods

To confirm that the implemented spike-triggered stimulation system is working properly, a peristimulus time histogram and spike-triggered average of the local field potential were examined. To investigate the changes in the neural connectivity after the spike-triggered stimulation, field-field, spike-field, and partial spike-field coherence were calculated in overlapping windows of 0.4 s, with step size 0.2 s, using the multi-taper method with 5 tapers and time-bandwidth parameter of 3 (Bokil et al., 2010) in the pre-stim and post-stim action exploration tasks. All sessions were integrated into the coherence analysis by averaging the spectrum and cross spectrum across all of the trials and the sessions, rather than averaging the final coherence values from each session. Since the action exploration task included two different classes—moving up the arm and getting a tactile stimulus on the

neck—the coherence values were computed for each of these classes separately. For spike-field coherence and partial spike-field coherence, we used only those channels with a firing rate of over 0.1 Hz in all sessions for both spike and LFP measurements, to take only stable channels into the calculation. The resulting coherence values were all z-scored based on the previous research (Jarvis & Mitra, 2001) to easily visualize the statistical significance.

The spike time tiling coefficient (STTC) was also computed and compared to explore the changes after the spike-triggered stimulation. Delta-t of 0.05 second was used for the analysis, although other values of delta-t were also explored to confirm the consistent pattern. Although STTC itself can reduce the bias from the firing rate and pattern (Cutts & Eglen, 2014), we removed the channels with significant changes in firing rate distribution ($p<0.05$ in rank-sum test) to minimize the bias, and removed the channels that had no spikes in any of the runs. To focus on the channel pairs with significant changes in STTC rather than the whole population, the number of outliers with significant changes in STTC after stimulation was compared between the spike-triggered stimulation and the random and no stimulation conditions based on rank-sum test. For identifying outliers, a threshold of 3 standard deviations was used. The same analysis was also used for negative and positive outliers as well, to see whether the stimulation was more effective for increasing or decreasing STTC values.

4.3. Results

4.3.1. Functional connectivity between SMG and S1 during different actions

To find the behavioral tasks that can stably activate the functional connectivity between SMG and S1, field-field coherence during action exploration tasks was analyzed. Figure 4.2A–4.2E shows the averaged field-field coherence (z-scored) between SMG and S1 during different action classes. During all the action classes, the average coherence showed a peak in low-frequency range, which was in low beta range (12–16 Hz). The coherence during motor imagery, regardless of its type, was generally lower than that during tactile stimuli or an actual execution of the movement. Among different types of tactile stimuli, touches on the cheek and neck yielded the highest field-field coherence, followed by shoulder, arm, and hand. This is consistent with the subject's residual sensations, since he has intact sensations on his face and neck, and some residual sensations on his shoulder and arm. For imagined and executed movements, the classes with the highest coherence are: moving the head, imagining moving the elbow, moving the elbow, moving the shoulder, and the rest of imagined movements (head and shoulder).

Figure 4.2F, on the other hand, shows the number of channel pairs with significant field-field coherence ($p<0.05$ after multiple testing corrections with Benjamini-Hochberg procedure), instead of the average magnitude of the coherence. Tactile stimuli, except for the touch on the hand, generally had the largest number of channel pairs with significant coherence. Actual motor output, except for moving the shoulder, also showed a comparable number of such channel pairs. Other actions, such as motor imagery and imagined reach, had relatively lower field-field coherence. Based on these results, we selected lifting the arm up and tactile stimuli on the neck for the following experiments, and used the neural activity recorded during such actions to quantify the functional connectivity.

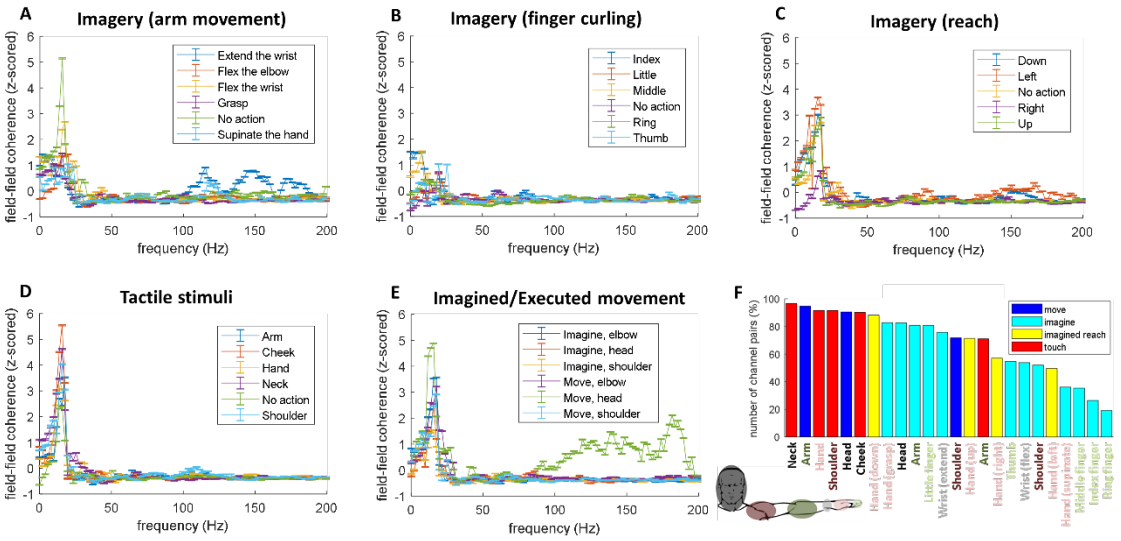

Figure 4.2 Field-field coherence between SMG and S1 during different actions. A-E) Z-scored field-field coherence between SMG and S1 during different action classes, averaged across all the channel pairs. F) The number of channel pairs with significant field-field coherence ($p<0.05$, multiple testing corrected; Benjamini-Hochberg procedure).

4.3.2. Implementation of spike-triggered stimulation system

To investigate the performance of the spike-triggered stimulation system, the spike-triggered average LFP in SMG was examined. The spikes and LFPs measured in the selected channel in SMG that was triggering stimulation in S1 during the task was used to plot spike-triggered average LFP in Figure 4.3A, which shows a stimulation artifact 20 ms after the spike. This demonstrates that the system was successfully delivering the stimulation at the specified time points. The same lag can be also found in Figure 4.3B, which shows the distribution of the time lag between the spikes and the stimulation. The stimulation is mostly focused at around 20 ms after the spike.

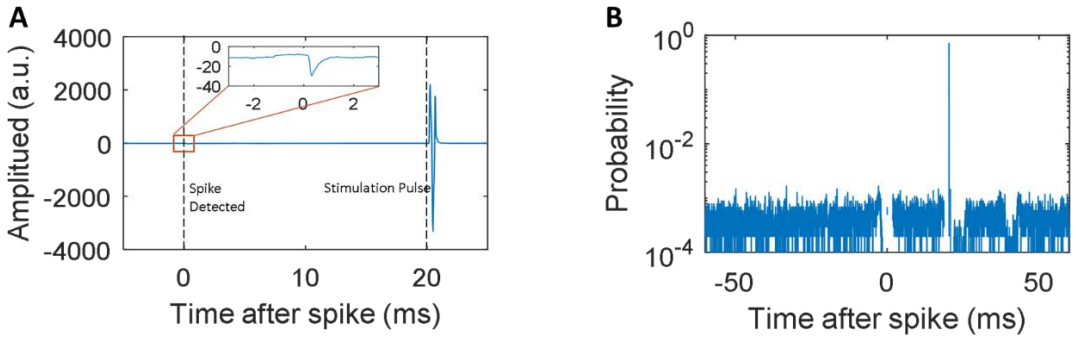

Figure 4.3. Performance of spike-triggered stimulation system. Detected spikes and corresponding stimulation outputs. B) Distribution of the time lag between spikes and stimulations during spike-triggered stimulations.

4.3.3. Changes in STTC after stimulation

The changes in functional connectivity between SMG and S1 after stimulation were assessed based on STTC. Figure 4.4A shows the distribution of the changes in STTC in three conditions: spike-triggered stimulation, random stimulation, and no stimulation. All three conditions had similar distributions, except for the large number of positive outliers in spike-triggered stimulation condition. The rank-sum test comparing the spike-triggered stimulation against random stimulation and no stimulation condition showed significant p-values ($p<0.0005$ and $p<0.05$, respectively), whereas the distributions from random stimulation and no stimulation conditions were not significantly different (rank-sum test, $p>0.05$).

The result of the rank-sum test, however, can be confounded by the main distribution, not the number of outliers found in Figure 4A. Therefore, we also compared the number of outliers in each condition (Figure 4B–D). Figure 4B shows the distribution of the number of outliers in STTC changes, with the threshold of three standard deviations. All the distributions were significantly different from each other with $p<0.05$ (rank-sum test), but the spike-triggered stimulation was more significantly different from the other two conditions ($p<0.0001$, rank-sum test).

Figure 4.4C and 4.4D also present the distribution of the number of outliers, but with negative (Figure 4.4C) and positive (Figure 4.4D) outliers

separately. Compared to the other two conditions, the spike-triggered stimulation did not show significantly different distribution for negative outliers, but it did show significant p-values with positive outliers in a rank-sum test comparing random stimulation conditions ($p<0.005$). This demonstrates that the spike-triggered stimulation has increased the number of outliers with significant increase in STTC, rather than significant decrease in STTC.

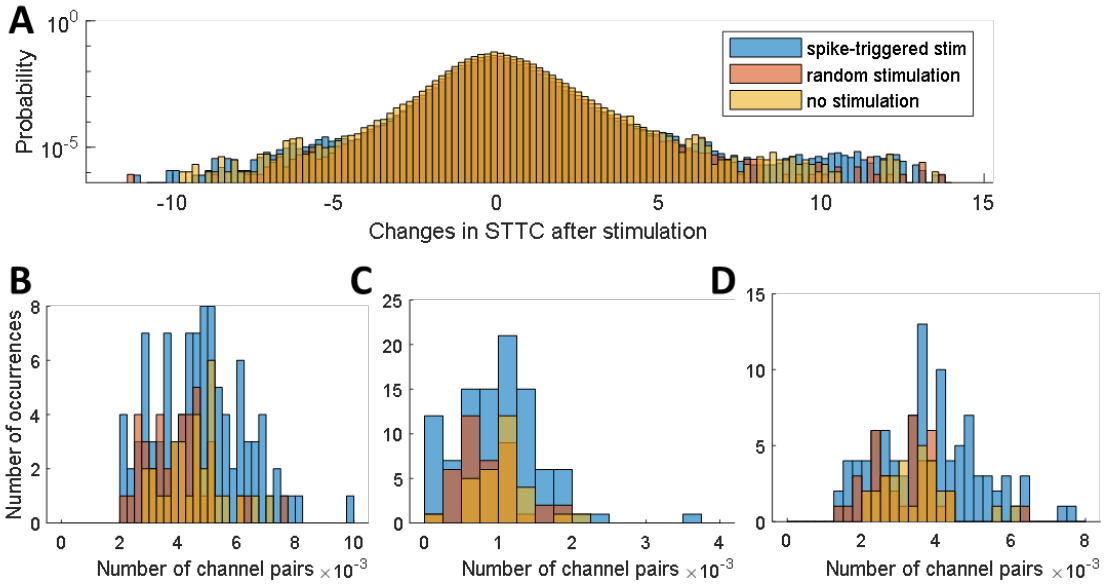

Figure 4.4. Changes in STTC after spike-triggered stimulation. A) Distribution of changes in STTC in three different conditions: spike-triggered stimulation (blue), random stimulation (red), and no stimulation (yellow). The spike-triggered stimulation condition showed a significantly different distribution compared to the other two conditions ($p<0.0005$ for random stimulation, $p<0.05$ for no stimulation; rank-sum test). B–D) Distribution of the number of all outliers (B), negative outliers (C), and positive outliers (D) in STTC changes, with a threshold of three standard deviations.

4.3.4. Changes in partial spike-field coherence within S1 after stimulation

To investigate any effect of stimulation on the functional connectivity within the stimulated area, the changes in the partial spike-field coherence within S1 were also investigated. Figure 4.5A shows the population averaged partial spike-field coherence, measured from all the possible channel pairs within S1. Each panel corresponds to different action classes used in the experiment: moving the arm (left) and getting tactile stimuli on the neck (right). Each color comes from different runs of the action exploration task, where two of them are before the stimulation (pre-stim1 and 2), and the other one is after the stimulation (post-stim). The data shown in the figure was from no stimulation condition only, so there was no stimulation delivered in between pre-stims and post-stim for this data set. There are no significant differences between coherences in different runs of the action exploration task, which demonstrates the consistency of the data in the population level. Another thing to note here is that tactile stimuli on the subject's neck led to high partial spike-field coherence in the low-frequency range, namely in the theta and delta bands, which was not shown during motor output on the arm area. Both conditions, however, had a shared peak around the alpha and low-beta range. Since the highest coherence was achieved in the delta and theta range during tactile stimuli, we chose theta to be analyzed in the following analysis.

Figure 4.5B shows the distribution of changes in partial spike-field coherence in the theta band after the stimulation, measured while the subject was moving his arm up (left) or getting tactile stimuli on his neck (right). In both cases, the changes in coherence after the spike-triggered stimulation were significantly different from random and no stimulation, but they were more significant during tactile stimuli on the neck ($p = 0.0012$ and $1.6 \times 10\text{-}4$ for spike-triggered stimulation vs. random and no stimulation during moving up the arm; $p = 3.8 \times 10\text{-}6$ and $6.6 \times 10\text{-}23$ for the same test during tactile stimuli on the neck; both from Kruskal-Wallis test). Between no stimulation and random stimulation, the distributions of coherence changes were not significantly different during moving up the arm ($p = 0.26$; Kruskal-Wallis test), but they were significant during tactile stimuli on the neck ($p = 6.9 \times 10\text{-}12$; Kruskal-Wallis test).

Figure 4.5C shows scatter plots comparing changes in partial spike-field coherence against the phase of the coherence measured before the stimulation, with four different stimulation conditions (each of the columns), and during different actions (each of the rows). As presented in the histogram in Figure 4.5B, spike-triggered stimulation and random stimulation led to larger changes in partial spike-field coherence in the theta band within S1, measured while the subject was getting tactile stimuli on his neck. The changes in the coherence were in both directions, and most of the channel pairs with large changes were from those with zero phase in partial spike-field coherence in pre-stim recordings. Such large changes were not

observed in no stimulation condition and between pre-stim recordings, which looks at the changes in the coherence between two pre-stim recordings rather than between pre-stim and post-stim recordings.

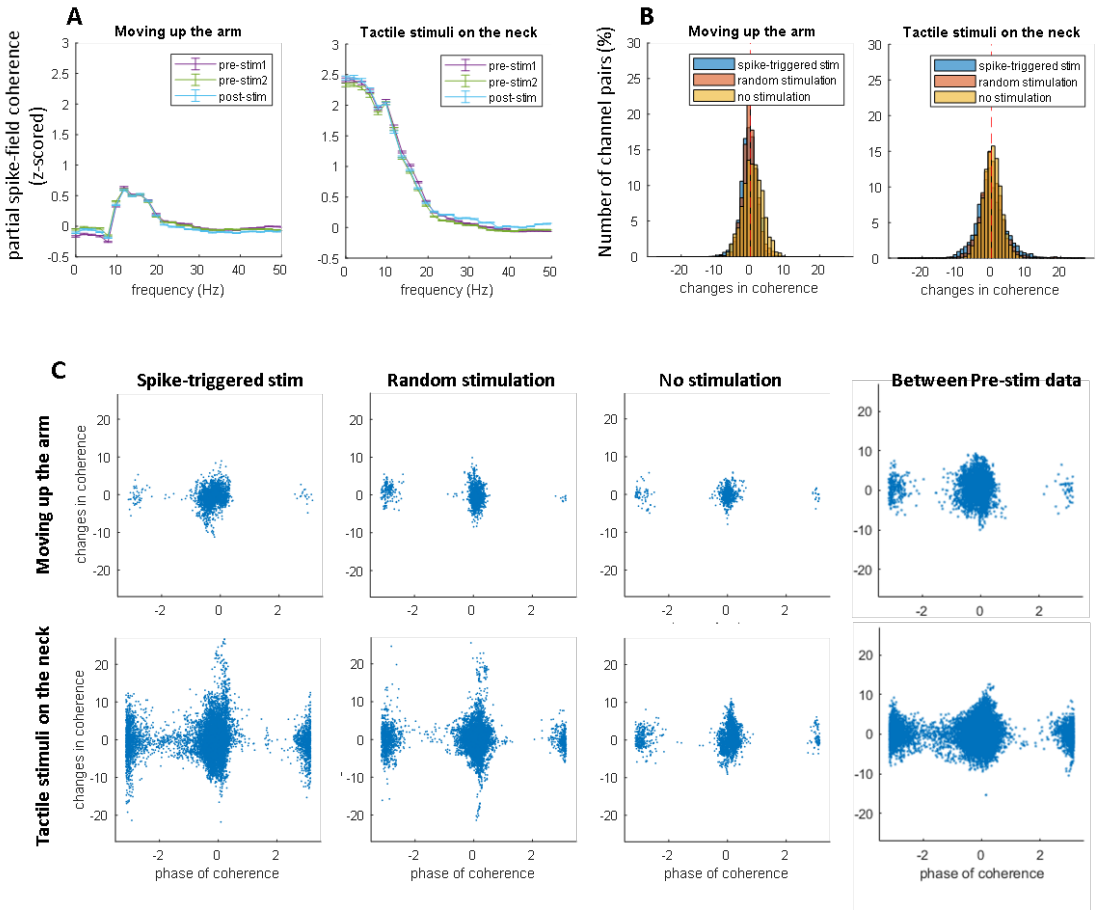

Figure 4.5. Partial spike-field coherence within S1. A) Population-averaged partial spike-field coherence, while the subject was moving his arm up (left), and while he was receiving tactile stimuli on his neck (right). Each color corresponds to different runs of the action exploration task, which is two runs before the stimulation (pre-stim1 and 2), and another run after the stimulation (post-stim). To show the consistency of the data, this only shows no stimulation condition. B) Distribution of the changes in partial spike-field coherence in the theta band in each stimulation condition (spike-triggered stimulation, random stimulation, and no stimulation), for each action class (moving up the arm, and receiving tactile stimuli on the neck). C) Scatter plots showing the changes in partial spike-field coherence after stimulation with respect to the phase of the coherence in the pre-stim recordings. The top row is while the subject was moving his arm, and the bottom row is when the subject was getting tactile stimuli on his neck. Each column corresponds to aforementioned stimulation conditions, with an additional column showing the changes of coherence between two pre-stim data, which is equivalent to no stimulation condition except for the different lag between the recordings.

4.4. Discussion

In this study, we implemented a closed-loop stimulation system that delivers stimulation in S1 in response to recorded spikes in a single channel of SMG. The lag between the spikes and the onset of the stimulation pulses could be specified, and the constancy of such a lag was demonstrated. With the lag of 20 ms between spikes and the stimulation, we could find population-level changes in STTC between spikes in both areas, and also in partial spike-field coherence between channels within S1. For STTC, the spike-triggered stimulation could increase the number of outliers with significant changes in STTC, especially the positive outliers, compared to no stimulation and random stimulation condition. For partial spike-field coherence within the stimulated region, both spike-triggered stimulation and random stimulation could increase the variance of the changes in coherence, compared to no stimulation condition.

One interesting point here is that we used 20 ms of lag between spikes and stimulations, which is at the longer end of the range that has been previously reported to induce a long-term potentiation in a cell culture (Bi & Poo, 2001). This might be due to multisynaptic connections in the channel pairs used in our experiment. The previous studies on spike time-dependent plasticity were based on spike-triggered stimulationa between the neurons with monosynaptic connections. However, in our experiment, we could not find channel pairs with electrophysiological evidence that suggests monosynaptic connections, such as low synaptic latency and low synaptic jitter (Doyle & Andresen, 2001).

Therefore, the lag between stimulations and spikes that is known to be optimal for strengthening the connectivity in monosynaptic connections might be too short to work in the polysynaptic connections. Also, although 20 ms of lag was selected based on the pilot study comparing the connectivity during the subject's rest before and after the spike-triggered stimulation with different lags (data not shown), it might be suboptimal since the recording was not paired with a behavioral task that can yield stable and strong functional connectivity. Hence, further investigation on the effect of different lags between spikes and stimulations with the same task structure as in our study (i.e. neural recording during a behavioral task before and after the spike-triggered stimulation) would be necessary.

We also found population-level changes in connectivity rather than changes in the connectivity between specific pairs of channels. Since we stimulated a few channels in S1 based on the spikes recorded in a selected channel in SMG, changes in connectivity between the recording channel and the stimulated channels were expected after spike-triggered stimulation as shown in the previous study in monkeys (Jackson et al., 2006). However, we could only find population-level changes in STTC and partial spike-field coherence. This might be due to second-order connection from the recording channel and stimulated area. As mentioned above, 20ms of lag between stimulations and spikes is at the longer end of the range that has been shown to strengthen monosynaptic connections (Bi & Poo, 2001). If it is longer than the optimal lag for

strengthening the connections between the channel pair we targeted in the experiment, there is a chance that the connection from the recording channel to another channel in SMG to the stimulation channel is more prone to change the connectivity; since it takes more time for the action potential to arrive at the stimulated channel, there will be a higher chance of concurrently activating synapsis during the depolarization of neurons in the stimulated area, which is the mechanism of spike timing-dependent plasticity shown in cellular studies (Dan & Poo, 2004; Jackson et al., 2006). In this hypothetical situation, the connectivity between the channels in stimulated area and some channels in recording areas that have high connectivity with the recording channel can be more susceptible to plasticity.

Another possible reason for finding population-level changes in connectivity is due to different types of neurons. Choosing channel pairs between SMG and S1 with the highest partial spike-field coherence does not necessarily mean that these channel pairs are more prone to change connectivity after closed-loop stimulation. There might be some other channel pairs that are more likely to change the connectivity between them. For example, in the hippocampus, long-term potentiation requires postsynaptic burst firing (Kampa et al., 2007). If the same principle applies for parietal regions as well, then the neurons with burst firing in S1, rather than the neurons that were directly stimulated, might show a larger increase in connectivity with SMG channels.

Population-level changes were also found in partial spike-field coherence within stimulated regions, which might be due to large spread of electrical stimulation in the area: instead of stimulating a very local area of the brain, the stimulation might have been delivered in a much larger area, leading to a population-level changes in connectivity in the stimulated area. Another interesting finding in the partial spike-field coherence was that such population-level changes did not occur in the same direction; the coherence increased in some channel pairs, decreased in some other channel pairs, and in most of the cases, it stayed around the same value. Although the stimulation was delivered at the same time, this suggests that the different synapses may have a different effect from the stimulation. It has been shown in the previous study with an intracortical stimulation that the same stimulation pattern can lead to both potentiation and suppression of cortical excitability, depending on the brain region and the individuals (Keller et al., 2018). Although its mechanism is not found yet, such different responses in cortical excitability might be one of the reasons why we found changes in partial spike-field coherence in both directions after stimulation.

Although there are many aspects to investigate further, our study demonstrates the possibility of artificially changing connectivity with stimulation in the human brain. In the case of stroke, for example, artificial connection can provide a bridge in a damaged cortical area, which can facilitate rehabilitation. There are also several movement disorders that can benefit from functional reorganization

through stimulation (Jackson et al., 2006; Nudo et al., 1996; Raineteau & Schwab, 2001). Hence, our study provides a good starting point for studying the effect of stimulation on neural connectivity, which will ultimately help people with neurological diseases.

Chapter 5

COGNITIVE MODULATION OF SINGLE-CHANNEL FIRING RATE

5.1. Introduction

For human cortical stimulation, there are several parameters that can be programmed independently, such as amplitude, frequency, and location of the stimulation. Our previous research has shown that these independent parameters can affect evoked sensations, and that the same set of stimulation parameters does not necessarily yield the same sensation every time (Armenta Salas et al., 2018). Therefore, prior to stimulation, these parameters must be mapped for each channel, and the percepts generated by each parameter set should be characterized. The process of changing the parameters of each stimulus and recording the subject's verbal description is tedious and time consuming. On the other hand, by having the subject calibrate and explore the parameters via closed-loop bidirectional BMI, parameter mapping could be substantially more efficient.

One possible way to achieve such a self-calibration system for stimulation parameters is by using the activity of single neuron for controlling each of parameters. It has been shown that the activity of single neurons can be volitionally controlled both in monkey (Fetz, 1969, 2007) and human studies (Aflalo et al., 2015), and can be used to calibrate stimulation parameters in muscles to activate the muscle groups in a desired way (Moritz et al., 2008).

To demonstrate this, here we show the possibility of volitional control of the firing rate recorded in a single channel. Without even notifying the participants of a mental imagery they have to use to control a single-channel activity, they could increase or decrease the neuronal firing rate of a single channel in the supramarginal gyrus (SMG) or anterior intraparietal area (AIP) to reach specific rates and maintain that rate for 0.3–0.5 seconds. This shows the possibility of using the participants' single-channel activity to cognitively control their own spike-contingent stimulation to engage in the operation of a closed-loop bidirectional BMI system.

5.2. Methods

5.2.1. Subject

Two tetraplegic patients have participated in the study. Subject EGS was a male tetraplegic patient, who was 32 years old, 10 years post-lesion at the time of implantation. He had a complete C3/C4 spinal cord injury, which led to paralysis of all limbs. Subject FG, on the other hand, was a 32-year-old male tetraplegic patient who was 1.5 years post-injury at the point of recruitment for a clinical trial of a BMI system with intracortical recording and stimulation. He suffered a complete C5/C6 spinal cord injury, but has some residual sensation in his upper arm (anterior-radial section and posterior-radial section) and forearm. All experimental procedures for both

patients were reviewed and approved by the Institutional Review Boards (IRB) of the University of Southern California (USC) and Rancho Los Amigos National Rehabilitation Hospital (RLA). The implantation of the electrodes was done at Keck Hospital of USC, and the study sessions were held at RLA for EGS, and RLA and the patient's house for FG.

5.2.2. Experimental setup

All the tasks were performed while the subjects were seated in their wheel chair (at RLA) or on their bed (at the patient's house). The tasks were displayed on a 27-inch LCD monitor in a lit room using Psychophysics Toolbox (Brainard, 1997) for MATLAB.

5.2.3. Experimental design

In order to examine the subjects' ability to control single-channel activity and explore the possibility of using it for self-calibration of stimulation parameters, three behavioral tasks were conducted: an action exploration task, biofeedback circle task, and biofeedback bar task (Figure 5.1). First, in action exploration task, we cued one of four behaviors: open and closed grip (for grasping), scratching the back of the head, windmill (for rotating the arm), and counting (for counting numbers in the head). In a preliminary training block (action

exploration task), subjects imagined performing cued behaviors during an action phase (Figure 5.1A). Threshold crossing (TC) rates (i.e., unsorted spike firing rates) from these training data were examined to identify channels whose TC rates modulated with regard to the imagined action. One of these channels was selected as the control source, and its TC rates (normalized to the mean TC rates during the training) were shown graphically as size of a circle (biofeedback circle task) or length of a bar (biofeedback bar task). In both tasks, the effector started at a neutral position (corresponding to the mean TC rates), and targets appeared which would require the subject to modulate the TC rates higher or lower than the mean (Figure 5.1B-C). In the biofeedback circle task, TC rates above the mean made the circle effector bigger, and the TC rates lower than the mean made the circle effector smaller. In the biofeedback bar task TC rates above the mean caused the bar to move to the right, whereas TC rates lower than the mean caused the bar to move to the left. To evaluate the subjects' volitional control over single-channel TC rates, the subject had to reach and hold on a target for 0.3 seconds (circle) and 0.5 seconds (bar). In the biofeedback circle task, the effector simply had to be in the extreme of the indicated target (bigger than targets outside the neutral size, or smaller than targets within the neutral size). In the biofeedback bar task, however, the cursor had to remain within a constrained target area. This, in addition to having four different target locations rather than two, made the biofeedback bar task more

challenging and supported more detailed evaluation of the subjects' ability to modulate single-channel TC rates.

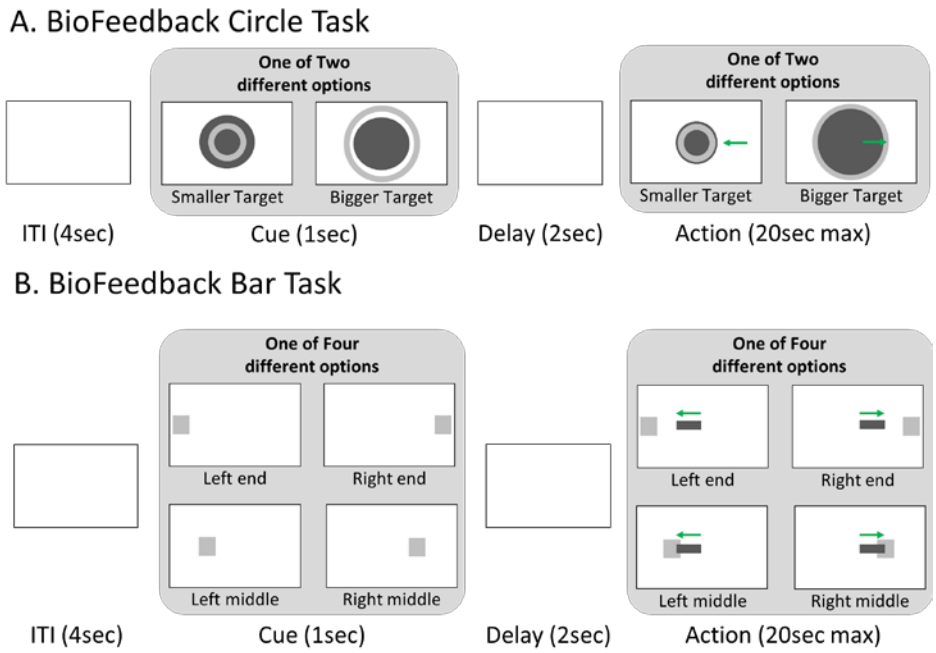

Figure 5.1. Design of BioFeedback task. A) BioFeedback circle task, in which the subject has to increase or decrease the size of the cursor (dark gray circle) by changing the spike firing rate of a single channel, to reach the target (light gray ring). B) BioFeedback bar task. The subject also has to reach the target (light gray rectangle) by moving the cursor (dark gray bar) with single-channel firing rate as in the biofeedback circle task, but it has four different locations for the target. Also, the subject has to reach the target and stay there for half a second to move on to the next trial.

5.2.4. Signal recording

Subject EGS was implanted with two 96-channel, platinum-tipped Neuroport microelectrode recording arrays (Blackrock Microsystems, Salt Lake City, UT) in AIP and BA5. The microelectrodes in each of the arrays were 1.5 mm long, and arranged in a 10-by-10 grid with 400-μm spacing. Preoperative fMRI tasks following the protocols described in (Aflalo et al., 2015) were used for surgical planning.

Subject FG was implanted with the same Neuroport arrays in SMG and PMv, with additional two 7-by-7 sputtered iridium oxide film (SIROF)-tipped microelectrode arrays in S1. Preoperative fMRI tasks based on our previous research (Aflalo et al., 2015) were also used to identify these brain areas for surgical planning, with additional tasks described in (Armenta Salas et al., 2018) to identify the location of S1.

5.2.5. Statistics and analysis methods

A t-test was applied to compare TC rates between action classes in the action exploration task and identify which channel would be used in the biofeedback task. Multiple comparison correction was not used in the online task because channels were selected based on an ordering of p-values, not their absolute values. The p-values were corrected for multiple comparison

in offline analysis, however, to ensure they were significant. Holm-Bonferroni method was used, with false-discovery rate less than 0.05 (Holm, 1979).

For both the biofeedback circle and bar tasks, the TC rates of the selected channel was examined during each trial to assess whether the subject exerted volitional control. The success rate in the task in each session for each of the target locations was also examined.

5.3. Results

5.3.1. Population level tuning

With 44 and 18 sessions of the action exploration task with EGS and FG, respectively, we found a population of channels tuned to each of the action classes (Figure 5.2A-B). Here, we focused on threshold crossings (i.e., unsorted spike firing rates) because sorting was not applied online. On average, each of the action classes had about four and 47 tuned channels in EGS and FG, after summing up the number of tuned channels across both arrays. FG had at least 14 tuned channels for each action in each session, and EGS had at least one channel for at least one action class throughout the sessions, allowing us to use it for the control in the biofeedback task. At the time of the first experiment, EGS has been implanted for about four years,

with degraded signal-to-noise ratio, whereas for FG it was less than two months. This may explain the significant difference in the number of tuned channels between EGS and FG.

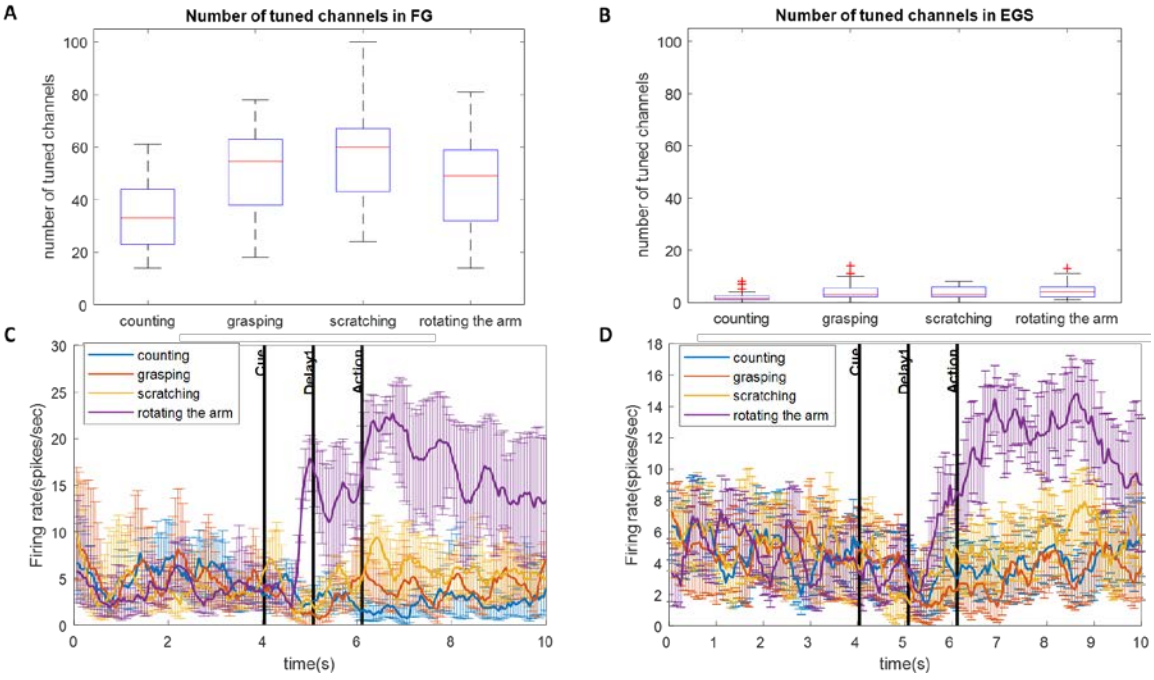

Figure 5.2. Results from action exploration task. A-B) Number of the channels tuned to each of the action classes used in action exploration task, in FG and EGS. C-D) Example firing activity of tuned unit.

5.3.2. Subject's ability to volitionally control neural activity

Both in FG and EGS, the size of the cursor during the biofeedback circle task was well controlled to reach the target (Figure 5.4A and 5.D). The firing rates of the single channel selected to control the cursor size were also well associated with the target size, as shown in Figure 5.1B and E. The success

rate was 100% for both targets in FG, whereas in EGS it was 83.3% on average. EGS showed a better performance for increasing the firing rate rather than for decreasing it, with success rate of 94.9% and 71.8% for a bigger target and smaller target, respectively.

Results from biofeedback bar task also showed FG and EGS's fine control over single-channel TC rates: TC rates from a selected channel was well controlled to reach and hold the target for 0.5 seconds (Figure 5.5A, B, D, and E). As the biofeedback bar task requires finer control of single-channel activity than the biofeedback circle task, performance was relatively worse for the bar task than circle task. However, both FG and EGS could still get the target in more than 40% of the trials on average (Figure 5.5C and F).

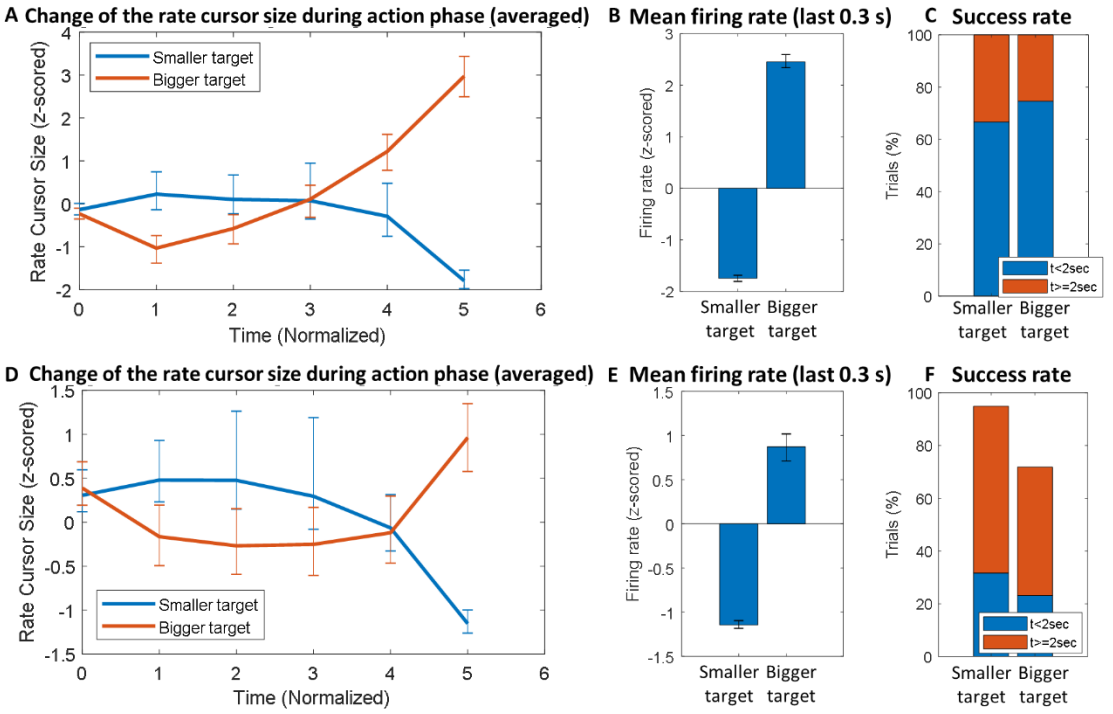

Figure 5.3. Results from biofeedback circle task. A–C) Results from FG's biofeedback circle tasks, showing the session-averaged cursor size during action phase (A), mean firing rate during the last 0.3 seconds of the trial (B), and success rate for each target size, bigger and smaller target (C). In C, each color shows a portion of the trials that were completed within two seconds (blue), and after two seconds since the action onset. D-F) The same set of figures with the results from the biofeedback task, with EGS' data.

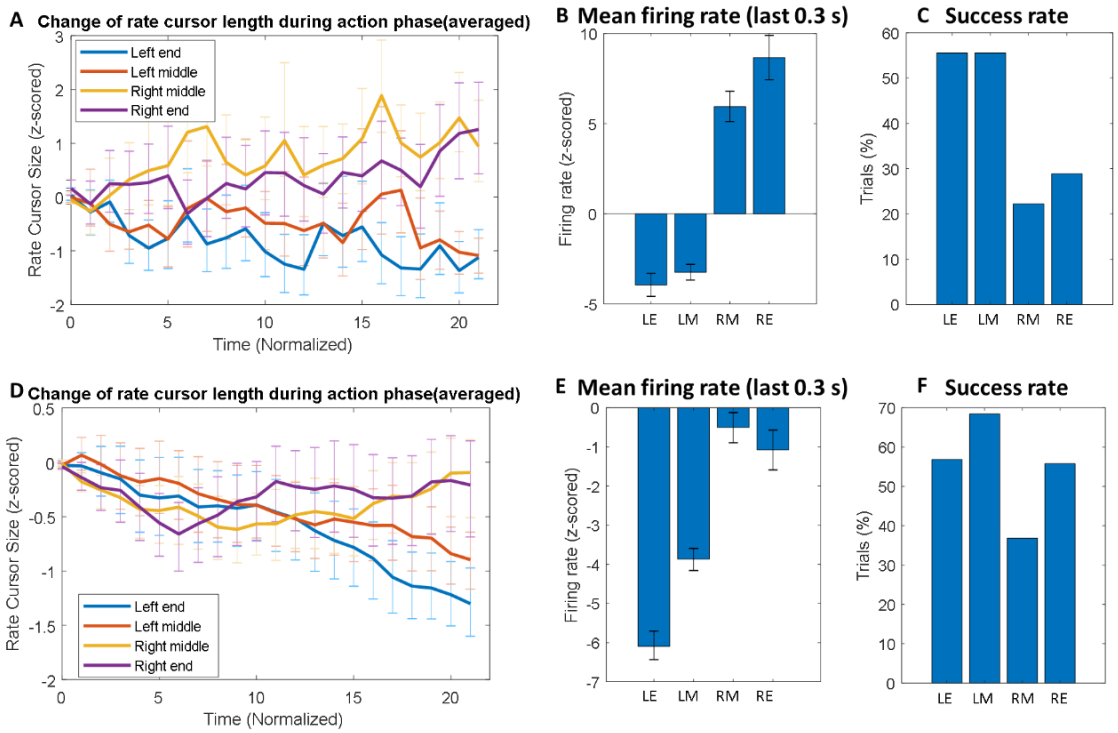

Figure 5.4. Results from biofeedback bar task. A–C) Results from FG's biofeedback bar tasks, showing the session-averaged cursor length during action phase (A), mean firing rate during the last 0.3 seconds of the trial (B), and success rate for each target location: left end (LE), left middle (LM), right middle (RM), and right end (RE) (C). D-F) The same set of figures with the results from biofeedback task, with EGS' data.

5.4. Discussion

In this study, we demonstrated the subjects' ability to volitionally control a single-channel activity. In SMG, PMv, AIP, and BA5, we could find the channels tuned to different mental imagery such as grasping, rotating the arm, and scratching the back of the head, and to counting numbers in the mind. On average, counting numbers had the least number of tuned channels compared to

other mental imagery, which is consistent with the literature showing that SMG, PMv, AIP, and BA5 are responsible for the arm and hand movements (Aflalo et al., 2015; Andres et al., 2017; Brandi et al., 2014; Fabbri et al., 2016; Johnson-Frey et al., 2005; Klaes et al., 2015; Kroliczak & Frey, 2009; Rozzi et al., 2008).

The subject could find one of such imagery to control a firing rate in the selected channel to reach certain level of activity, even without knowing which imagery the selected channel was tuned to. Such controllability of a single-channel activity is consistent with our previous research on volitional control of AIP and BA5 activity with imagined arm movements in humans (Aflalo et al., 2015), and with monkey studies on single-unit control (Fetz, 1969, 2007). Interestingly, the subjects could not only choose the general direction of changes in the firing rate, but also could maintain the firing rate in a certain range for a short duration of time. Based on the subjects' report, it could be done with a few different mental strategies, such as changing the speed or the force of imagined action and changing the level of focus on the imagery. The subjects also tried exploring different mental strategies that were not used before, such as reaching or touching other parts of the body, to finely control the firing rate in a selected channel.

As for controllability, both of the participants found it easier to reach the targets by reducing the firing rate rather than increasing it. For the biofeedback bar task, for example, both of them showed a better average performance for reaching the

targets on the left, which requires lowering the firing rates, rather than the targets on the right. The same pattern was found in a biofeedback circle task with EGS, whereas FG showed a slightly better performance for increasing the firing rate instead, which is the opposite of the aforementioned trend. It might be due to different bias we have found in the firing rate recorded from FG and EGS. FG, for example, suffered from a bias toward a higher firing rate. In Figure 5.3B, the absolute value of the z-scored firing rate at the end of the trial with bigger targets, which requires an increased firing rate, is larger than that of the firing rate for smaller target, which needs a decreased firing rate. It is even more prominent in Figure 5.4B, as the decreased firing rate (z-scored) is not as low as -5 whereas the increased firing rate easily exceeds 5. Indeed, the subject has reported that when he tried to increase the firing rate, it usually overshot and he had to decrease it back. The same issue does not apply to the biofeedback circle task, since the subject only has to increase the firing rate above a certain threshold, but it can be problematic in the biofeedback bar task that requires the subject to hold the increased firing rate in a certain range; hence, better performance for increasing the firing rate in biofeedback circle task, and worse performance for increasing the rate in biofeedback bar task. EGS, however, suffered from the bias toward lower firing rate, which is shown clearly in Figure 4E—even for the right targets that need a higher firing rate, EGS could not increase the z-scored firing rate above 0. Hence, he showed a worse performance for increasing the firing rate for both the biofeedback bar and circle task.

Although further investigation is necessary, such a different pattern in bias might be due to different signal quality and mean firing rate. As mentioned earlier, at the time of the first experiment, it has been more than 4 years since EGS got implanted. FG, on the other hand, got implanted 2 months prior to the first experiment in our study. This led to significantly lower signal-to-noise ratio and average firing rates in EGS, which might be one of the reasons why EGS experienced a difficulty increasing the firing rate. Since the signal from FG had higher signal-to-noise ratio and mean firing rate, FG did not experience such a problem. Instead, because increasing the firing rate has no ceiling effect, unlike reducing the firing rate which has minimum value of 0 Hz, FG found it much easier to increase the firing rate, which made the firing rate overshoot. However, it still does not fully explain the bias, since the firing rate was z-scored based on the mean and standard deviation of previous recordings. Therefore, the bias in firing rates toward certain directions might reflect a shifted mean firing rate. Changes in the units and their mean firing rates can occur in a short period of time (Degenhart et al., 2020; Nuyujukian et al., 2014), but because it happened in a specific direction for each of the participants repeatedly, it would be worth investigating.

Despite the necessity of further investigation, this study demonstrates the possibility of using single-channel activity recorded in parietal area for a control. For example, it can be connected to stimulation parameters in bidirectional BMIs, so that the subject can calibrate and explore the stimulation pattern. As it

uses the firing rate recorded in a single channel, it also has a possibility of multiplexing by connecting multiple channels' activity to multiple parameters of stimulation. Future work would be necessary to implement such a self-calibration system and explore the possibility of volitionally controlling multiple channels independently.

Chapter 6

CONCLUSION

In this dissertation, we explored the applications of bidirectional BMI. In Chapter 3, we investigated the connectivity between supramarginal gyrus (SMG) and PMv (ventral premotor area), and also between anterior intraparietal (AIP) and Brodmann's area 5 (BA5), which can provide a great starting point for studying connectivity changes after closed-loop stimulation through bidirectional BMI. By using different types of behavioral tasks such as imagining/executing movements, receiving tactile stimuli, and counting numbers, which include motor components, sensory components, and none of these components, respectively, we figured out which connections get activated during which task. We also revealed that the spikes in PMv may drive the activity in SMG during motor output, sensory input, and counting numbers. This allows us to understand the functional connections between the areas in parietal regions in depth, and help us establish the baseline for studying neural connectivity and a closed-loop stimulation scheme for changing it, which was discussed in Chapter 4.

In Chapter 4, we demonstrated the possibility of using a spike-triggered stimulation system, which can be implemented with a bidirectional BMI, for inducing neural plasticity. By delivering stimulations in one area every time the spikes are recorded from another area, we showed that the connectivity between those areas can increase on a population-level. In addition to this, we also found evidence that stimulating a

certain area, even if it is not triggered by the firing activity in another area, can alter the connectivity within the stimulated area. To the best of our knowledge, it is the first evidence of artificial changes in neural connectivity through spike-triggered stimulation.

Chapter 4 is about how the stimulation changes brain connectivity. In contrast, Chapter 5 is about how we can use the neural signal to change the stimulation. In this chapter, we showed the possibility of using the neural activity for the calibration of stimulation pattern, by demonstrating fine, volitional control of the single-channel firing rate. We found tuned channels for certain motor imagery in SMG, PMv, AIP, and BA5, and the subjects could use proper mental imagery to volitionally control the single-channel firing rate from these areas. The subjects were able to increase and decrease the single-channel firing rate to reach a certain level, and also could hold it within a given range for a short duration of time. Although further study is necessary, this demonstrates the potential for self-calibration and optimization of stimulation parameters in bidirectional BMI.

Taken together, the work presented here shows the applications of bidirectional BMI: Chapter 3 establishes the baseline connectivity between brain areas, Chapter 4 demonstrates how we can alter such connectivity through stimulation using bidirectional BMI, and Chapter 5 suggests an idea of changing the stimulation pattern by neural activity. A lot of BMIs have been developed as a unidirectional system: motor BMI, for example, allowed the subjects to control robotic limb with their neural activity, but only with a visual feedback (Potter, 2010). However, people are

now developing bidirectional BMIs which may bring great advances not only in the performance of motor BMIs through tactile feedback, but also in our understanding of dynamical properties of neural systems (Potter, 2010). For motor BMI with tactile feedback, for example, even though a chronic implantation of microelectrode arrays in humans for miscrostimulation was done only in recent studies (Armenta Salas et al., 2018; Flesher et al., 2016), the improved performance of BMI-based robotic arm control through tactile feedback by stimulation has already been shown (Flesher et al., 2021). Likewise, the work presented here also demonstrates great advances that bidirectional BMI can bring not only to the people suffering from tetraplegia, stroke, and other neurological disorders, but also to the neuroscientists studying neural dynamics, through its broad applications.

BIBLIOGRAPHY

Aflalo, T., Kellis, S., Klaes, C., Lee, B., Shi, Y., Pejsa, K., Shanfield, K., Hayes-Jackson, S., Aisen, M., Heck, C., Liu, C., & Andersen, R. A. (2015). Neurophysiology. Decoding motor imagery from the posterior parietal cortex of a tetraplegic human. *Science (New York, N.Y.)*, *348*(6237), 906–910. https://doi.org/10.1126/science.aaa5417

Ajiboye, A. B., Willett, F. R., Young, D. R., Memberg, W. D., Murphy, B. A., Miller, J. P., Walter, B. L., Sweet, J. A., Hoyen, H. A., Keith, M. W., Peckham, P. H., Simeral, J. D., Donoghue, J. P., Hochberg, L. R., & Kirsch, R. F. (2017). Restoration of reaching and grasping movements through brain-controlled muscle stimulation in a person with tetraplegia: A proof-of-concept demonstration. *The Lancet*, *389*(10081), 1821–1830. https://doi.org/10.1016/S0140-6736(17)30601-3

Andersen, R. A., Andersen, K. N., Hwang, E. J., & Hauschild, M. (2014). Optic ataxia: From Balint's syndrome to the parietal reach region. *Neuron*, *81*(5), 967–983. https://doi.org/10.1016/j.neuron.2014.02.025

Andres, M., Pelgrims, B., Olivier, E., & Vannuscorps, G. (2017). The left supramarginal gyrus contributes to finger positioning for object use: A neuronavigated transcranial magnetic stimulation study. *European Journal of Neuroscience*, *46*(12), 2835–2843. https://doi.org/10.1111/ejn.13763

Armenta Salas, M., Bashford, L., Kellis, S., Jafari, M., Jo, H., Kramer, D., Shanfield, K., Pejsa, K., Lee, B., Liu, C. Y., & Andersen, R. A. (2018). Proprioceptive and cutaneous sensations in humans elicited by intracortical microstimulation. *ELife*, *7*, e32904. https://doi.org/10.7554/eLife.32904

Arroyo, S., Lesser, R. P., Gordon, B., Uematsu, S., Jackson, D., & Webber, R. (1993). Functional significance of the mu rhythm of human cortex: An electrophysiologic study with subdural electrodes. *Electroencephalography and Clinical Neurophysiology*, *87*(3), 76–87. https://doi.org/10.1016/0013-4694(93)90114-B

Ban, H., Barrett, G., Borisevich, A., Chaturvedi, A., Dahle, J., Dehghani, H., DoValle, B., Dubois, J., Field, R., Gopalakrishnan, V., Gundran, A., Henninger, M., Ho, W., Hughes, H., Jin, R., Kates-Harbeck, J., Landy, T., Lara, A., Leggiero, M., & Zhu, Z. (2021). *Kernel Flow: A high channel count scalable TD-fNIRS system*. 23. https://doi.org/10.1117/12.2582888

Basser, P. J. (1995). Inferring microstructural features and the physiological state of tissues from diffusion-weighted images. *NMR in Biomedicine*, *8*(7), 333–344. https://doi.org/10.1002/nbm.1940080707

Basser, P. J., Pajevic, S., Pierpaoli, C., Duda, J., & Aldroubi, A. (2000). In vivo fiber tractography using DT-MRI data. *Magnetic Resonance in Medicine*, *44*(4), 625–632. https://doi.org/10.1002/1522-2594(200010)44:4<625::aid-mrm17>3.0.co;2-o

Bastos, A. M., & Schoffelen, J.-M. (2016). A Tutorial Review of Functional Connectivity Analysis Methods and Their Interpretational Pitfalls. *Frontiers in Systems Neuroscience*, *0*. https://doi.org/10.3389/fnsys.2015.00175

Bhagat, N. A., Venkatakrishnan, A., Abibullaev, B., Artz, E. J., Yozbatiran, N., Blank, A. A., French, J., Karmonik, C., Grossman, R. G., O'Malley, M. K., Francisco, G. E., & Contreras-Vidal, J. L. (2016). Design and Optimization of an EEG-Based Brain Machine Interface (BMI) to an Upper-Limb Exoskeleton for Stroke Survivors. *Frontiers in Neuroscience*, *0*. https://doi.org/10.3389/fnins.2016.00122

Bi, G., & Poo, M. (2001). Synaptic Modification by Correlated Activity: Hebb's Postulate Revisited. *Annual Review of Neuroscience*, *24*(1), 139–166. https://doi.org/10.1146/annurev.neuro.24.1.139

Bliss, T. V., & Lomo, T. (1973). Long-lasting potentiation of synaptic transmission in the dentate area of the anaesthetized rabbit following stimulation of the perforant path. *The Journal of Physiology*, *232*(2), 331–356. https://doi.org/10.1113/jphysiol.1973.sp010273

Bokil, H., Andrews, P., Kulkarni, J. E., Mehta, S., & Mitra, P. P. (2010). Chronux: A platform for analyzing neural signals. *Journal of Neuroscience Methods*, *192*(1), 146–151. https://doi.org/10.1016/j.jneumeth.2010.06.020

Bouton, C. E., Shaikhouni, A., Annetta, N. V., Bockbrader, M. A., Friedenberg, D. A., Nielson, D. M., Sharma, G., Sederberg, P. B., Glenn, B. C., Mysiw, W. J., Morgan, A. G., Deogaonkar, M., & Rezai, A. R. (2016). Restoring cortical control of functional movement in a human with quadriplegia. *Nature*, *533*(7602), 247–250. https://doi.org/10.1038/nature17435

Bowyer, S. M. (2016). Coherence a measure of the brain networks: Past and present. *Neuropsychiatric Electrophysiology*, *2*(1), 1. https://doi.org/10.1186/s40810-015-0015-7

Brainard, D. H. (1997). The Psychophysics Toolbox. *Spatial Vision*, *10*(4), 433–436.

Brandi, M.-L., Wohlschläger, A., Sorg, C., & Hermsdörfer, J. (2014). The Neural Correlates of Planning and Executing Actual Tool Use. *Journal of Neuroscience*, *34*(39), 13183–13194. https://doi.org/10.1523/JNEUROSCI.0597-14.2014

Buchholz, V. N., Jensen, O., & Medendorp, W. P. (2014). Different roles of alpha and beta band oscillations in anticipatory sensorimotor gating. *Frontiers in Human Neuroscience*, *0*. https://doi.org/10.3389/fnhum.2014.00446

Burge, J., Girshick, A. R., & Banks, M. S. (2010). Visual–Haptic Adaptation Is Determined by Relative Reliability. *The Journal of Neuroscience*, *30*(22), 7714–7721. https://doi.org/10.1523/JNEUROSCI.6427-09.2010

Buzsáki, G., & Wang, X.-J. (2012). Mechanisms of gamma oscillations. *Annual Review of Neuroscience*, *35*, 203–225. https://doi.org/10.1146/annurev-neuro-062111-150444

Caporale, N., & Dan, Y. (2008). Spike timing-dependent plasticity: A Hebbian learning rule. *Annual Review of Neuroscience*, *31*, 25–46. https://doi.org/10.1146/annurev.neuro.31.060407.125639

Carmena, J. M., Lebedev, M. A., Crist, R. E., O'Doherty, J. E., Santucci, D. M., Dimitrov, D. F., Patil, P. G., Henriquez, C. S., & Nicolelis, M. A. L. (2003). Learning to Control a Brain–Machine Interface for Reaching and Grasping by Primates. *PLOS Biology*, *1*(2), e42. https://doi.org/10.1371/journal.pbio.0000042

Chen, R., Yaseen, Z., Cohen, L. G., & Hallett, M. (1998). Time course of corticospinal excitability in reaction time and self-paced movements. *Annals of Neurology*, *44*(3), 317–325. https://doi.org/10.1002/ana.410440306

Cheyne, D. O. (2013). MEG studies of sensorimotor rhythms: A review. *Experimental Neurology*, *245*, 27–39. https://doi.org/10.1016/j.expneurol.2012.08.030

Chiappalone, M., Bove, M., Vato, A., Tedesco, M., & Martinoia, S. (2006). Dissociated cortical networks show spontaneously correlated activity patterns during in vitro

development. *Brain Research*, *1093*(1), 41–53. https://doi.org/10.1016/j.brainres.2006.03.049

Coenen, A., Fine, E., & Zayachkivska, O. (2014). Adolf Beck: A forgotten pioneer in electroencephalography. *Journal of the History of the Neurosciences*, *23*(3), 276–286. https://doi.org/10.1080/0964704X.2013.867600

Collinger, J. L., Wodlinger, B., Downey, J. E., Wang, W., Tyler-Kabara, E. C., Weber, D. J., McMorland, A. J. C., Velliste, M., Boninger, M. L., & Schwartz, A. B. (2013). High-performance neuroprosthetic control by an individual with tetraplegia. *Lancet (London, England)*, *381*(9866), 557–564. https://doi.org/10.1016/S0140-6736(12)61816-9

Colombo, M., & Weinberger, N. (2018). Discovering Brain Mechanisms Using Network Analysis and Causal Modeling. *Minds and Machines*, *28*(2), 265–286. https://doi.org/10.1007/s11023-017-9447-0

Cutts, C. S., & Eglen, S. J. (2014). Detecting pairwise correlations in spike trains: An objective comparison of methods and application to the study of retinal waves. *The Journal of Neuroscience: The Official Journal of the Society for Neuroscience*, *34*(43), 14288–14303. https://doi.org/10.1523/JNEUROSCI.2767-14.2014

Dadarlat, M. C., O'Doherty, J. E., & Sabes, P. N. (2015). A learning-based approach to artificial sensory feedback leads to optimal integration. *Nature Neuroscience*, *18*(1), 138–144. https://doi.org/10.1038/nn.3883

Dan, Y., & Poo, M.-M. (2004). Spike timing-dependent plasticity of neural circuits. *Neuron*, *44*(1), 23–30. https://doi.org/10.1016/j.neuron.2004.09.007

Degenhart, A. D., Bishop, W. E., Oby, E. R., Tyler-Kabara, E. C., Chase, S. M., Batista, A. P., & Yu, B. M. (2020). Stabilization of a brain–computer interface via the alignment of low-dimensional spaces of neural activity. *Nature Biomedical Engineering*, *4*(7), 672–685. https://doi.org/10.1038/s41551-020-0542-9

Dehorter, N., Vinay, L., Hammond, C., & Ben-Ari, Y. (2012). Timing of developmental sequences in different brain structures: Physiological and pathological implications. *European Journal of Neuroscience*, *35*(12), 1846–1856. https://doi.org/10.1111/j.1460-9568.2012.08152.x

Diamond, M. C., Krech, D., & Rosenzweig, M. R. (1964). The effects of an enriched environment on the histology of the rat cerebral cortex. *Journal of Comparative Neurology*, *123*(1), 111–119. https://doi.org/10.1002/cne.901230110

Dobelle, W. H., & Mladejovsky, M. G. (1974). Phosphenes produced by electrical stimulation of human occipital cortex, and their application to the development of a prosthesis for the blind. *The Journal of Physiology*, *243*(2), 553-576.1.

Doud, A. J., Lucas, J. P., Pisansky, M. T., & He, B. (2011). Continuous Three-Dimensional Control of a Virtual Helicopter Using a Motor Imagery Based Brain-Computer Interface. *PLOS ONE*, *6*(10), e26322. https://doi.org/10.1371/journal.pone.0026322

Dowling, J. (2005). Artificial human vision. *Expert Review of Medical Devices*, *2*(1), 73–85. https://doi.org/10.1586/17434440.2.1.73

Doyle, M. W., & Andresen, M. C. (2001). Reliability of monosynaptic sensory transmission in brain stem neurons in vitro. *Journal of Neurophysiology*, *85*(5), 2213–2223. https://doi.org/10.1152/jn.2001.85.5.2213

Ernst, M. O., & Banks, M. S. (2002). Humans integrate visual and haptic information in a statistically optimal fashion. *Nature*, *415*(6870), 429–433. https://doi.org/10.1038/415429a

Fabbri, S., Stubbs, K. M., Cusack, R., & Culham, J. C. (2016). Disentangling Representations of Object and Grasp Properties in the Human Brain. *Journal of Neuroscience*, *36*(29), 7648–7662. https://doi.org/10.1523/JNEUROSCI.0313-16.2016

Fetz, E. E. (1969). Operant conditioning of cortical unit activity. *Science (New York, N.Y.)*, *163*(3870), 955–958. https://doi.org/10.1126/science.163.3870.955

Fetz, E. E. (2007). Volitional control of neural activity: Implications for brain-computer interfaces. *The Journal of Physiology*, *579*(Pt 3), 571–579. https://doi.org/10.1113/jphysiol.2006.127142

Fetz, E. E., & Baker, M. A. (1973). Operantly conditioned patterns on precentral unit activity and correlated responses in adjacent cells and contralateral muscles. *Journal of Neurophysiology*, *36*(2), 179–204. https://doi.org/10.1152/jn.1973.36.2.179

Flesher, S. N., Collinger, J. L., Foldes, S. T., Weiss, J. M., Downey, J. E., Tyler-Kabara, E. C., Bensmaia, S. J., Schwartz, A. B., Boninger, M. L., & Gaunt, R. A. (2016). Intracortical microstimulation of human somatosensory cortex. *Science Translational Medicine*, *8*(361), 361ra141-361ra141. https://doi.org/10.1126/scitranslmed.aaf8083

Flesher, S. N., Downey, J. E., Weiss, J. M., Hughes, C. L., Herrera, A. J., Tyler-Kabara, E. C., Boninger, M. L., Collinger, J. L., & Gaunt, R. A. (2021). A brain-computer interface that evokes tactile sensations improves robotic arm control. *Science*, *372*(6544), 831–836. https://doi.org/10.1126/science.abd0380

Fogassi, L., Gallese, V., Fadiga, L., Luppino, G., Matelli, M., & Rizzolatti, G. (1996). Coding of peripersonal space in inferior premotor cortex (area F4). *Journal of Neurophysiology*, *76*(1), 141–157. https://doi.org/10.1152/jn.1996.76.1.141

Ganguly, K., & Poo, M. (2013). Activity-Dependent Neural Plasticity from Bench to Bedside. *Neuron*, *80*(3), 729–741. https://doi.org/10.1016/j.neuron.2013.10.028

Georgopoulos, A. P., Lurito, J. T., Petrides, M., Schwartz, A. B., & Massey, J. T. (1989). Mental rotation of the neuronal population vector. *Science (New York, N.Y.)*, *243*(4888), 234–236. https://doi.org/10.1126/science.2911737

Gilja, V., Nuyujukian, P., Chestek, C. A., Cunningham, J. P., Yu, B. M., Fan, J. M., Churchland, M. M., Kaufman, M. T., Kao, J. C., Ryu, S. I., & Shenoy, K. V. (2012). A high-performance neural prosthesis enabled by control algorithm design. *Nature Neuroscience*, *15*(12), 1752–1757. https://doi.org/10.1038/nn.3265

Gu, Y., Angelaki, D. E., & Deangelis, G. C. (2008). Neural correlates of multisensory cue integration in macaque MSTd. *Nature Neuroscience*, *11*(10), 1201–1210. https://doi.org/10.1038/nn.2191

Guggenmos, D. J., Azin, M., Barbay, S., Mahnken, J. D., Dunham, C., Mohseni, P., & Nudo, R. J. (2013). Restoration of function after brain damage using a neural prosthesis. *Proceedings of the National Academy of Sciences*, *110*(52), 21177–21182. https://doi.org/10.1073/pnas.1316885110

Hagmann, P., Cammoun, L., Gigandet, X., Meuli, R., Honey, C. J., Wedeen, V. J., & Sporns, O. (2008). Mapping the Structural Core of Human Cerebral Cortex. *PLoS Biology*, *6*(7), e159. https://doi.org/10.1371/journal.pbio.0060159

Harvey, C. D., Collman, F., Dombeck, D. A., & Tank, D. W. (2009). Intracellular dynamics of hippocampal place cells during virtual navigation. *Nature*, *461*(7266), 941–946. https://doi.org/10.1038/nature08499

He, Y., Eguren, D., Azorín, J. M., Grossman, R. G., Luu, T. P., & Contreras-Vidal, J. L. (2018). Brain–machine interfaces for controlling lower-limb powered robotic systems. *Journal of Neural Engineering*, *15*(2), 021004. https://doi.org/10.1088/1741-2552/aaa8c0

Henry, J. C. (2006). Electroencephalography: Basic Principles, Clinical Applications, and Related Fields, Fifth Edition. *Neurology*, *67*(11), 2092-2092-a. https://doi.org/10.1212/01.wnl.0000243257.85592.9a

Hochberg, L. R., Bacher, D., Jarosiewicz, B., Masse, N. Y., Simeral, J. D., Vogel, J., Haddadin, S., Liu, J., Cash, S. S., van der Smagt, P., & Donoghue, J. P. (2012). Reach and grasp by people with tetraplegia using a neurally controlled robotic arm. *Nature*, *485*(7398), 372–375. https://doi.org/10.1038/nature11076

Hochberg, L. R., Serruya, M. D., Friehs, G. M., Mukand, J. A., Saleh, M., Caplan, A. H., Branner, A., Chen, D., Penn, R. D., & Donoghue, J. P. (2006). Neuronal ensemble control of prosthetic devices by a human with tetraplegia. *Nature*, *442*(7099), 164–171. https://doi.org/10.1038/nature04970

Holm, S. (1979). A Simple Sequentially Rejective Multiple Test Procedure. *Scandinavian Journal of Statistics*, *6*(2), 65–70.

Hubel, D. H., & Wiesel, T. N. (1998). Early exploration of the visual cortex. *Neuron*, *20*(3), 401–412. https://doi.org/10.1016/s0896-6273(00)80984-8

Ito, M., & Kano, M. (1982). Long-lasting depression of parallel fiber-Purkinje cell transmission induced by conjunctive stimulation of parallel fibers and climbing fibers in the cerebellar cortex. *Neuroscience Letters*, *33*(3), 253–258. https://doi.org/10.1016/0304-3940(82)90380-9

Jackson, A., Mavoori, J., & Fetz, E. E. (2006). Long-term motor cortex plasticity induced by an electronic neural implant. *Nature*, *444*(7115), 56–60. https://doi.org/10.1038/nature05226

Jacobs, M., Premji, A., & Nelson, A. J. (2012). Plasticity-Inducing TMS Protocols to Investigate Somatosensory Control of Hand Function. *Neural Plasticity*, *2012*, e350574. https://doi.org/10.1155/2012/350574

Jarvis, M. R., & Mitra, P. P. (2001). Sampling Properties of the Spectrum and Coherency of Sequences of Action Potentials. *Neural Computation*, *13*(4), 717–749. https://doi.org/10.1162/089976601300014312

Johnson-Frey, S. H., Newman-Norlund, R., & Grafton, S. T. (2005). A distributed left hemisphere network active during planning of everyday tool use skills. *Cerebral Cortex (New York, N.Y.: 1991)*, *15*(6), 681–695. https://doi.org/10.1093/cercor/bhh169

Kampa, B. M., Letzkus, J. J., & Stuart, G. J. (2007). Dendritic mechanisms controlling spike-timing-dependent synaptic plasticity. *Trends in Neurosciences*, *30*(9), 456–463. https://doi.org/10.1016/j.tins.2007.06.010

Keller, C. J., Huang, Y., Herrero, J. L., Fini, M. E., Du, V., Lado, F. A., Honey, C. J., & Mehta, A. D. (2018). Induction and Quantification of Excitability Changes in Human

Cortical Networks. *Journal of Neuroscience*, *38*(23), 5384–5398. https://doi.org/10.1523/JNEUROSCI.1088-17.2018

Keller, T. A., & Just, M. A. (2016). Structural and functional neuroplasticity in human learning of spatial routes. *NeuroImage*, *125*, 256–266. https://doi.org/10.1016/j.neuroimage.2015.10.015

Kennedy, P. R., & Bakay, R. a. E. (1998). Restoration of neural output from a paralyzed patient by a direct brain connection. *NeuroReport*, *9*(8), 1707–1711.

Kennedy, P. R., Bakay, R. A. E., Moore, M. M., Adams, K., & Goldwaithe, J. (2000). Direct control of a computer from the human central nervous system. *IEEE Transactions on Rehabilitation Engineering*, *8*(2), 198–202. https://doi.org/10.1109/86.847815

Khanna, P., Totten, D., Novik, L., Roberts, J., Morecraft, R. J., & Ganguly, K. (2021). Low-frequency stimulation enhances ensemble co-firing and dexterity after stroke. *Cell*, *184*(4), 912-930.e20. https://doi.org/10.1016/j.cell.2021.01.023

Kim, S., Callier, T., Tabot, G. A., Gaunt, R. A., Tenore, F. V., & Bensmaia, S. J. (2015). Behavioral assessment of sensitivity to intracortical microstimulation of primate somatosensory cortex. *Proceedings of the National Academy of Sciences*, *112*(49), 15202–15207. https://doi.org/10.1073/pnas.1509265112

Kirkby, L. A., Sack, G. S., Firl, A., & Feller, M. B. (2013). A Role for Correlated Spontaneous Activity in the Assembly of Neural Circuits. *Neuron*, *80*(5), 1129–1144. https://doi.org/10.1016/j.neuron.2013.10.030

Klaes, C., Kellis, S., Aflalo, T., Lee, B., Pejsa, K., Shanfield, K., Hayes-Jackson, S., Aisen, M., Heck, C., Liu, C., & Andersen, R. A. (2015). Hand Shape Representations in the

Human Posterior Parietal Cortex. *Journal of Neuroscience*, *35*(46), 15466–15476. https://doi.org/10.1523/JNEUROSCI.2747-15.2015

Klaes, C., Shi, Y., Kellis, S., Minxha, J., Revechkis, B., & Andersen, R. A. (2014). A cognitive neuroprosthetic that uses cortical stimulation for somatosensory feedback. *Journal of Neural Engineering*, *11*(5), 056024. https://doi.org/10.1088/1741-2560/11/5/056024

Koivuniemi, A. S., & Otto, K. J. (2012). The depth, waveform and pulse rate for electrical microstimulation of the auditory cortex. *2012 Annual International Conference of the IEEE Engineering in Medicine and Biology Society*, 2489–2492. https://doi.org/10.1109/EMBC.2012.6346469

Kroliczak, G., & Frey, S. (2009). A Common Network in the Left Cerebral Hemisphere Represents Planning of Tool Use Pantomimes and Familiar Intransitive Gestures at the Hand-Independent Level. *Cerebral Cortex (New York, N.Y. : 1991)*, *19*, 2396–2410. https://doi.org/10.1093/cercor/bhn261

LaFleur, K., Cassady, K., Doud, A., Shades, K., Rogin, E., & He, B. (2013). Quadcopter control in three-dimensional space using a noninvasive motor imagery-based brain–computer interface. *Journal of Neural Engineering*, *10*(4), 046003. https://doi.org/10.1088/1741-2560/10/4/046003

Le Bihan, D., Mangin, J. F., Poupon, C., Clark, C. A., Pappata, S., Molko, N., & Chabriat, H. (2001). Diffusion tensor imaging: Concepts and applications. *Journal of Magnetic Resonance Imaging: JMRI*, *13*(4), 534–546. https://doi.org/10.1002/jmri.1076

Leocani, L., Toro, C., Zhuang, P., Gerloff, C., & Hallett, M. (2001). Event-related desynchronization in reaction time paradigms: A comparison with event-related

potentials and corticospinal excitability. *Clinical Neurophysiology*, *112*(5), 923–930. https://doi.org/10.1016/S1388-2457(01)00530-2

Linkenkaer-Hansen, K., Nikulin, V. V., Palva, S., Ilmoniemi, R. J., & Palva, J. M. (2004). Prestimulus Oscillations Enhance Psychophysical Performance in Humans. *Journal of Neuroscience*, *24*(45), 10186–10190. https://doi.org/10.1523/JNEUROSCI.2584-04.2004

MacLaren, E. J., Charlesworth, P., Coba, M. P., & Grant, S. G. N. (2011). Knockdown of mental disorder susceptibility genes disrupts neuronal network physiology in vitro. *Molecular and Cellular Neuroscience*, *47*(2), 93–99. https://doi.org/10.1016/j.mcn.2010.12.014

Markram, H., Gerstner, W., & Sjöström, P. J. (2011). A History of Spike-Timing-Dependent Plasticity. *Frontiers in Synaptic Neuroscience*, *0*. https://doi.org/10.3389/fnsyn.2011.00004

Markram, H., Lübke, J., Frotscher, M., & Sakmann, B. (1997). Regulation of synaptic efficacy by coincidence of postsynaptic APs and EPSPs. *Science (New York, N.Y.)*, *275*(5297), 213–215. https://doi.org/10.1126/science.275.5297.213

McFarland, D. J., Sarnacki, W. A., & Wolpaw, J. R. (2010). Electroencephalographic (EEG) control of three-dimensional movement. *Journal of Neural Engineering*, *7*(3), 036007. https://doi.org/10.1088/1741-2560/7/3/036007

McGuire, L. M. M., & Sabes, P. N. (2009). Sensory transformations and the use of multiple reference frames for reach planning. *Nature Neuroscience*, *12*(8), 1056–1061. https://doi.org/10.1038/nn.2357

Milekovic, T., Fischer, J., Pistohl, T., Ruescher, J., Schulze-Bonhage, A., Aertsen, A., Rickert, J., Ball, T., & Mehring, C. (2012). An online brain–machine interface using decoding of movement direction from the human electrocorticogram. *Journal of Neural Engineering*, *9*(4), 046003. https://doi.org/10.1088/1741-2560/9/4/046003

Miranda, R. A., Casebeer, W. D., Hein, A. M., Judy, J. W., Krotkov, E. P., Laabs, T. L., Manzo, J. E., Pankratz, K. G., Pratt, G. A., Sanchez, J. C., Weber, D. J., Wheeler, T. L., & Ling, G. S. F. (2015). DARPA-funded efforts in the development of novel brain–computer interface technologies. *Journal of Neuroscience Methods*, *244*, 52–67. https://doi.org/10.1016/j.jneumeth.2014.07.019

Moritz, C., Perlmutter, S., & Fetz, E. (2008). Direct control of paralysed muscles by cortical neurons. *Nature*, *456*, 639–642. https://doi.org/10.1038/nature07418

Musallam, S., Corneil, B. D., Greger, B., Scherberger, H., & Andersen, R. A. (2004). Cognitive Control Signals for Neural Prosthetics. *Science*, *305*(5681), 258–262. https://doi.org/10.1126/science.1097938

Nishimura, Y., Perlmutter, S. I., & Fetz, E. E. (2013). Restoration of upper limb movement via artificial corticospinal and musculospinal connections in a monkey with spinal cord injury. *Frontiers in Neural Circuits*, *7*, 57. https://doi.org/10.3389/fncir.2013.00057

Nudo, R. J. (2014). Plasticity of cerebral motor functions: Implications for repair and rehabilitation. In G. Kwakkel, L. Cohen, M. Selzer, R. Miller, & S. Clarke (Eds.), *Textbook of Neural Repair and Rehabilitation: Volume 1: Neural Repair and Plasticity* (2nd ed., Vol. 1, pp. 99–113). Cambridge University Press. https://doi.org/10.1017/CBO9780511995583.010

Nudo, R. J., Wise, B. M., SiFuentes, F., & Milliken, G. W. (1996). Neural substrates for the effects of rehabilitative training on motor recovery after ischemic infarct. *Science (New York, N.Y.)*, *272*(5269), 1791–1794. https://doi.org/10.1126/science.272.5269.1791

Nuyujukian, P., Kao, J. C., Fan, J. M., Stavisky, S. D., Ryu, S. I., & Shenoy, K. V. (2014). Performance sustaining intracortical neural prostheses. *Journal of Neural Engineering*, *11*(6), 066003. https://doi.org/10.1088/1741-2560/11/6/066003

O'Doherty, J. E., Lebedev, M. A., Ifft, P. J., Zhuang, K. Z., Shokur, S., Bleuler, H., & Nicolelis, M. A. L. (2011). Active tactile exploration using a brain–machine–brain interface. *Nature*, *479*(7372), 228–231. https://doi.org/10.1038/nature10489

Okun, M., Naim, A., & Lampl, I. (2010). The Subthreshold Relation between Cortical Local Field Potential and Neuronal Firing Unveiled by Intracellular Recordings in Awake Rats. *Journal of Neuroscience*, *30*(12), 4440–4448. https://doi.org/10.1523/JNEUROSCI.5062-09.2010

Pantev, C., Makeig, S., Hoke, M., Galambos, R., Hampson, S., & Gallen, C. (1991). Human auditory evoked gamma-band magnetic fields. *Proceedings of the National Academy of Sciences of the United States of America*, *88*(20), 8996–9000. https://doi.org/10.1073/pnas.88.20.8996

Personius, K. E., Chang, Q., Mentis, G. Z., O'Donovan, M. J., & Balice-Gordon, R. J. (2007). Reduced gap junctional coupling leads to uncorrelated motor neuron firing and precocious neuromuscular synapse elimination. *Proceedings of the National Academy of Sciences*, *104*(28), 11808–11813. https://doi.org/10.1073/pnas.0703357104

Pfurtscheller, G. (1992). Event-related synchronization (ERS): An electrophysiological correlate of cortical areas at rest. *Electroencephalography and Clinical Neurophysiology*, *83*(1), 62–69. https://doi.org/10.1016/0013-4694(92)90133-3

Pfurtscheller, G., & Aranibar, A. (1979). Evaluation of event-related desynchronization (ERD) preceding and following voluntary self-paced movement. *Electroencephalography and Clinical Neurophysiology*, *46*(2), 138–146. https://doi.org/10.1016/0013-4694(79)90063-4

Pfurtscheller, G., & Lopes da Silva, F. H. (1999). Event-related EEG/MEG synchronization and desynchronization: Basic principles. *Clinical Neurophysiology: Official Journal of the International Federation of Clinical Neurophysiology*, *110*(11), 1842–1857. https://doi.org/10.1016/s1388-2457(99)00141-8

Pfurtscheller, G., & McFarland, D. J. (2012). BCIs That Use Sensorimotor Rhythms. In *Brain–Computer Interfaces*. Oxford University Press. https://doi.org/10.1093/acprof:oso/9780195388855.003.0013

Pfurtscheller, G., & Neuper, C. (1997). Motor imagery activates primary sensorimotor area in humans. *Neuroscience Letters*, *239*(2–3), 65–68. https://doi.org/10.1016/s0304-3940(97)00889-6

Pfurtscheller, G., Neuper, C., Brunner, C., & da Silva, F. L. (2005). Beta rebound after different types of motor imagery in man. *Neuroscience Letters*, *378*(3), 156–159. https://doi.org/10.1016/j.neulet.2004.12.034

Pfurtscheller, G., Stancák, A., & Neuper, Ch. (1996). Event-related synchronization (ERS) in the alpha band — an electrophysiological correlate of cortical idling: A review.

International Journal of Psychophysiology, *24*(1), 39–46. https://doi.org/10.1016/S0167-8760(96)00066-9

Pineda, J. A. (2005). The functional significance of mu rhythms: Translating “seeing” and “hearing” into “doing.” *Brain Research Reviews*, *50*(1), 57–68. https://doi.org/10.1016/j.brainresrev.2005.04.005

Pistohl, T., Ball, T., Schulze-Bonhage, A., Aertsen, A., & Mehring, C. (2008). Prediction of arm movement trajectories from ECoG-recordings in humans. *Journal of Neuroscience Methods*, *167*(1), 105–114. https://doi.org/10.1016/j.jneumeth.2007.10.001

Pistohl, T., Schulze-Bonhage, A., Aertsen, A., Mehring, C., & Ball, T. (2012). Decoding natural grasp types from human ECoG. *NeuroImage*, *59*(1), 248–260. https://doi.org/10.1016/j.neuroimage.2011.06.084

Potter, S. M. (2010). Closing the Loop Between Neurons and Neurotechnology. *Frontiers in Neuroscience*, *0*. https://doi.org/10.3389/fnins.2010.00015

Rahman, A., Reato, D., Arlotti, M., Gasca, F., Datta, A., Parra, L. C., & Bikson, M. (2013). Cellular effects of acute direct current stimulation: Somatic and synaptic terminal effects. *The Journal of Physiology*, *591*(10), 2563–2578. https://doi.org/10.1113/jphysiol.2012.247171

Raineteau, O., & Schwab, M. E. (2001). Plasticity of motor systems after incomplete spinal cord injury. *Nature Reviews. Neuroscience*, *2*(4), 263–273. https://doi.org/10.1038/35067570

Ramón y Cajal, S. (1913). *Estudios sobre la degeneración y regeneración del sistema nervioso*. Hijos de Nicolás Moza.

Ranade, G., Ganguly, K., & Carmena, J. (2009, April 29). *LFP Beta Power Predicts Cursor Stationarity In BMI Task*. 4th International IEEE/EMBS Conference on Neural Engineering, 2009. NER '09. https://www.microsoft.com/en-us/research/publication/lfp-beta-power-predicts-cursor-stationarity-bmi-task/

Romo, R., Hernández, A., Zainos, A., Brody, C. D., & Lemus, L. (2000). Sensing without Touching: Psychophysical Performance Based on Cortical Microstimulation. *Neuron*, *26*(1), 273–278. https://doi.org/10.1016/S0896-6273(00)81156-3

Romo, R., Hernández, A., Zainos, A., & Salinas, E. (1998). Somatosensory discrimination based on cortical microstimulation. *Nature*, *392*(6674), 387–390. https://doi.org/10.1038/32891

Rozzi, S., Ferrari, P. F., Bonini, L., Rizzolatti, G., & Fogassi, L. (2008). Functional organization of inferior parietal lobule convexity in the macaque monkey: Electrophysiological characterization of motor, sensory and mirror responses and their correlation with cytoarchitectonic areas. *The European Journal of Neuroscience*, *28*(8), 1569–1588. https://doi.org/10.1111/j.1460-9568.2008.06395.x

Sainburg, R. L., Poizner, H., & Ghez, C. (1993). Loss of proprioception produces deficits in interjoint coordination. *Journal of Neurophysiology*, *70*(5), 2136–2147. https://doi.org/10.1152/jn.1993.70.5.2136

Sanes, J. N., & Donoghue, J. P. (2000). Plasticity and Primary Motor Cortex. *Annual Review of Neuroscience*, *23*(1), 393–415. https://doi.org/10.1146/annurev.neuro.23.1.393

Santhanam, G., Ryu, S. I., Yu, B. M., Afshar, A., & Shenoy, K. V. (2006). A high-performance brain–computer interface. *Nature*, *442*(7099), 195–198. https://doi.org/10.1038/nature04968

Schalk, G., Miller, K. J., Anderson, N. R., Wilson, J. A., Smyth, M. D., Ojemann, J. G., Moran, D. W., Wolpaw, J. R., & Leuthardt, E. C. (2008). Two-dimensional movement control using electrocorticographic signals in humans. *Journal of Neural Engineering*, *5*(1), 75–84. https://doi.org/10.1088/1741-2560/5/1/008

Serruya, M. D., Hatsopoulos, N. G., Paninski, L., Fellows, M. R., & Donoghue, J. P. (2002). Instant neural control of a movement signal. *Nature*, *416*(6877), 141–142. https://doi.org/10.1038/416141a

Simani, M. C., McGuire, L. M. M., & Sabes, P. N. (2007). Visual-shift adaptation is composed of separable sensory and task-dependent effects. *Journal of Neurophysiology*, *98*(5), 2827–2841. https://doi.org/10.1152/jn.00290.2007

Sober, S. J., & Sabes, P. N. (2005). Flexible strategies for sensory integration during motor planning. *Nature Neuroscience*, *8*(4), 490–497. https://doi.org/10.1038/nn1427

Song, W., Kerr, C. C., Lytton, W. W., & Francis, J. T. (2013). Cortical Plasticity Induced by Spike-Triggered Microstimulation in Primate Somatosensory Cortex. *PLOS ONE*, *8*(3), e57453. https://doi.org/10.1371/journal.pone.0057453

Sporns, O. (2007). Brain connectivity. *Scholarpedia*, *2*(10), 4695. https://doi.org/10.4249/scholarpedia.4695

Sporns, O., Tononi, G., & Kötter, R. (2005). The Human Connectome: A Structural Description of the Human Brain. *PLOS Computational Biology*, *1*(4), e42. https://doi.org/10.1371/journal.pcbi.0010042

Stanley, G. B., Li, F. F., & Dan, Y. (1999). Reconstruction of Natural Scenes from Ensemble Responses in the Lateral Geniculate Nucleus. *Journal of Neuroscience*, *19*(18), 8036–8042. https://doi.org/10.1523/JNEUROSCI.19-18-08036.1999

Stetson, C., & Andersen, R. A. (2014). The Parietal Reach Region Selectively Anti-Synchronizes with Dorsal Premotor Cortex during Planning. *Journal of Neuroscience*, *34*(36), 11948–11958. https://doi.org/10.1523/JNEUROSCI.0097-14.2014

Tabot, G. A., Dammann, J. F., Berg, J. A., Tenore, F. V., Boback, J. L., Vogelstein, R. J., & Bensmaia, S. J. (2013). Restoring the sense of touch with a prosthetic hand through a brain interface. *Proceedings of the National Academy of Sciences*, *110*(45), 18279–18284. https://doi.org/10.1073/pnas.1221113110

Tallon-Baudry, null, & Bertrand, null. (1999). Oscillatory gamma activity in humans and its role in object representation. *Trends in Cognitive Sciences*, *3*(4), 151–162. https://doi.org/10.1016/s1364-6613(99)01299-1

Tan, D. W., Schiefer, M. A., Keith, M. W., Anderson, J. R., Tyler, J., & Tyler, D. J. (2014). A neural interface provides long-term stable natural touch perception. *Science Translational Medicine*, *6*(257), 257ra138. https://doi.org/10.1126/scitranslmed.3008669

Taylor, D. M., Tillery, S. I. H., & Schwartz, A. B. (2002). Direct cortical control of 3D neuroprosthetic devices. *Science (New York, N.Y.)*, *296*(5574), 1829–1832. https://doi.org/10.1126/science.1070291

Tchumatchenko, T., Geisel, T., Volgushev, M., & Wolf, F. (2011). Spike Correlations – What Can They Tell About Synchrony? *Frontiers in Neuroscience*, *5*, 68. https://doi.org/10.3389/fnins.2011.00068

van Beers, R. J., Sittig, A. C., & Gon, J. J. (1999). Integration of proprioceptive and visual position-information: An experimentally supported model. *Journal of Neurophysiology*, *81*(3), 1355–1364. https://doi.org/10.1152/jn.1999.81.3.1355

van Ede, F., Jensen, O., & Maris, E. (2010). Tactile expectation modulates pre-stimulus β-band oscillations in human sensorimotor cortex. *NeuroImage*, *51*(2), 867–876. https://doi.org/10.1016/j.neuroimage.2010.02.053

Verstynen, T., & Sabes, P. N. (2011). How each movement changes the next: An experimental and theoretical study of fast adaptive priors in reaching. *The Journal of Neuroscience: The Official Journal of the Society for Neuroscience*, *31*(27), 10050–10059. https://doi.org/10.1523/JNEUROSCI.6525-10.2011

Vidal, J. (1977). Real-time detection of brain events in EEG. *Proceedings of the IEEE*. https://doi.org/10.1109/PROC.1977.10542

Vidal, J. J. (1973). Toward Direct Brain-Computer Communication. *Annual Review of Biophysics and Bioengineering*, *2*(1), 157–180. https://doi.org/10.1146/annurev.bb.02.060173.001105

Vinck, M., Battaglia, F. P., Womelsdorf, T., & Pennartz, C. (2012). Improved measures of phase-coupling between spikes and the Local Field Potential. *Journal of Computational Neuroscience*, *33*(1), 53–75. https://doi.org/10.1007/s10827-011-0374-4

Wang, X.-J. (2010). Neurophysiological and computational principles of cortical rhythms in cognition. *Physiological Reviews*, *90*(3), 1195–1268. https://doi.org/10.1152/physrev.00035.2008

Wessberg, J., Stambaugh, C. R., Kralik, J. D., Beck, P. D., Laubach, M., Chapin, J. K., Kim, J., Biggs, S. J., Srinivasan, M. A., & Nicolelis, M. A. L. (2000). Real-time prediction of hand trajectory by ensembles of cortical neurons in primates. *Nature*, *408*(6810), 361+. Gale Academic OneFile.

Wolpaw, J. R., McFarland, D. J., Neat, G. W., & Forneris, C. A. (1991). An EEG-based brain-computer interface for cursor control. *Electroencephalography and Clinical Neurophysiology*, *78*(3), 252–259. https://doi.org/10.1016/0013-4694(91)90040-B

Womelsdorf, T., Schoffelen, J.-M., Oostenveld, R., Singer, W., Desimone, R., Engel, A. K., & Fries, P. (2007). Modulation of neuronal interactions through neuronal synchronization. *Science (New York, N.Y.)*, *316*(5831), 1609–1612. https://doi.org/10.1126/science.1139597

Wong, R. O. L., Meister, M., & Shatz, C. J. (1993). Transient period of correlated bursting activity during development of the mammalian retina. *Neuron*, *11*(5), 923–938. https://doi.org/10.1016/0896-6273(93)90122-8

Yanagisawa, T., Hirata, M., Saitoh, Y., Kishima, H., Matsushita, K., Goto, T., Fukuma, R., Yokoi, H., Kamitani, Y., & Yoshimine, T. (2012). Electrocorticographic control of a prosthetic arm in paralyzed patients. *Annals of Neurology*, *71*(3), 353–361. https://doi.org/10.1002/ana.22613

Zabielska-Mendyk, E., Francuz, P., Jaśkiewicz, M., & Augustynowicz, P. (2018). The Effects of Motor Expertise on Sensorimotor Rhythm Desynchronization during Execution and Imagery of Sequential Movements. *Neuroscience*, *384*, 101–110. https://doi.org/10.1016/j.neuroscience.2018.05.028

Zamora-López, G., Zhou, C., & Kurths, J. (2011). Exploring Brain Function from Anatomical Connectivity. *Frontiers in Neuroscience*, *0*. https://doi.org/10.3389/fnins.2011.00083

Zanos, S., Rembado, I., Chen, D., & Fetz, E. E. (2018). Phase-Locked Stimulation during Cortical Beta Oscillations Produces Bidirectional Synaptic Plasticity in Awake Monkeys. *Current Biology: CB*, *28*(16), 2515-2526.e4. https://doi.org/10.1016/j.cub.2018.07.009

Zapała, D., Zabielska-Mendyk, E., Augustynowicz, P., Cudo, A., Jaśkiewicz, M., Szewczyk, M., Kopiś, N., & Francuz, P. (2020). The effects of handedness on sensorimotor rhythm desynchronization and motor-imagery BCI control. *Scientific Reports*, *10*(1), 2087. https://doi.org/10.1038/s41598-020-59222-w

SUPPLEMENTARY DATA

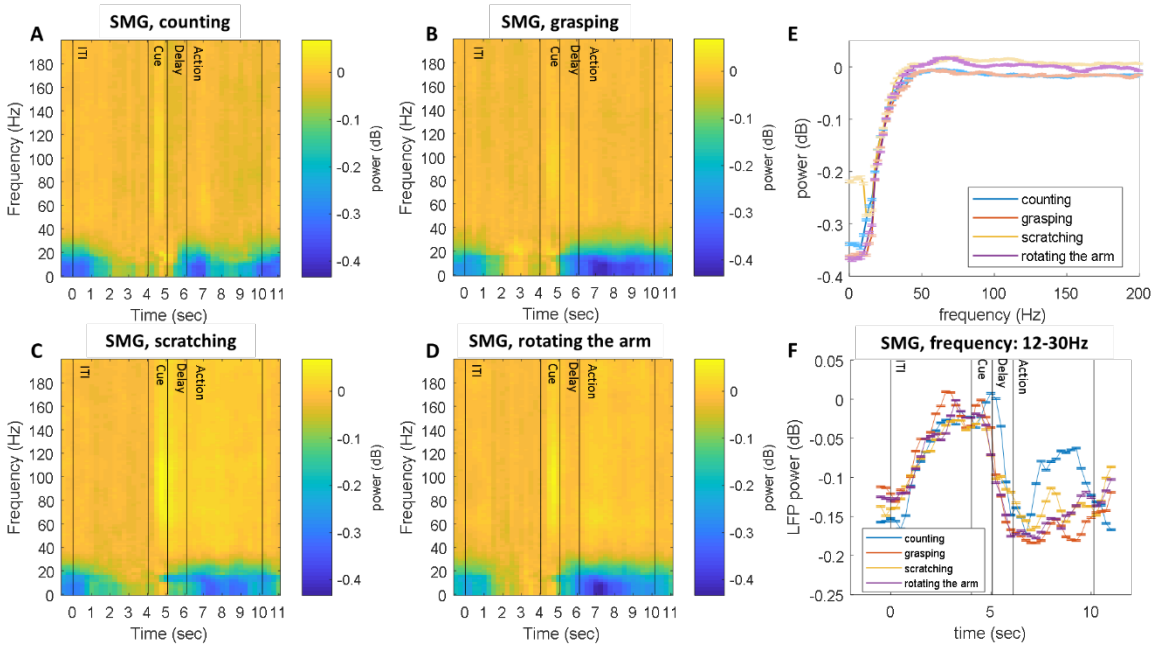

Figure S1. LFP power from SMG during action exploration task. A–D) Population averaged spectrogram from SMG during counting (A), grasping (B), scratching (C), and rotating the arm (D). E) Average LFP power in the first one-second window in the action phase (population averaged). F) Temporal changes in average LFP power in 12–30Hz (population averaged)

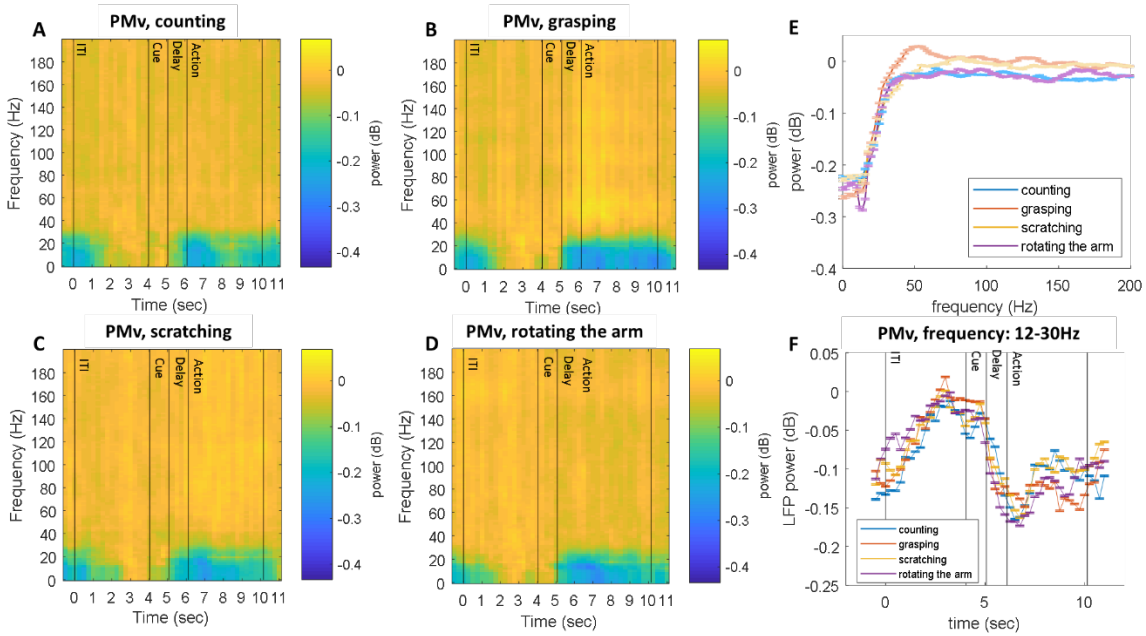

Figure S2. LFP power from PMv during action exploration task. A–D) Population-averaged spectrogram from PMv during counting (A), grasping (B), scratching (C), and rotating the arm (D). E) Average LFP power in the first one-second window in action phase (population averaged). F) Temporal changes in average LFP power in 12–30Hz (population averaged).

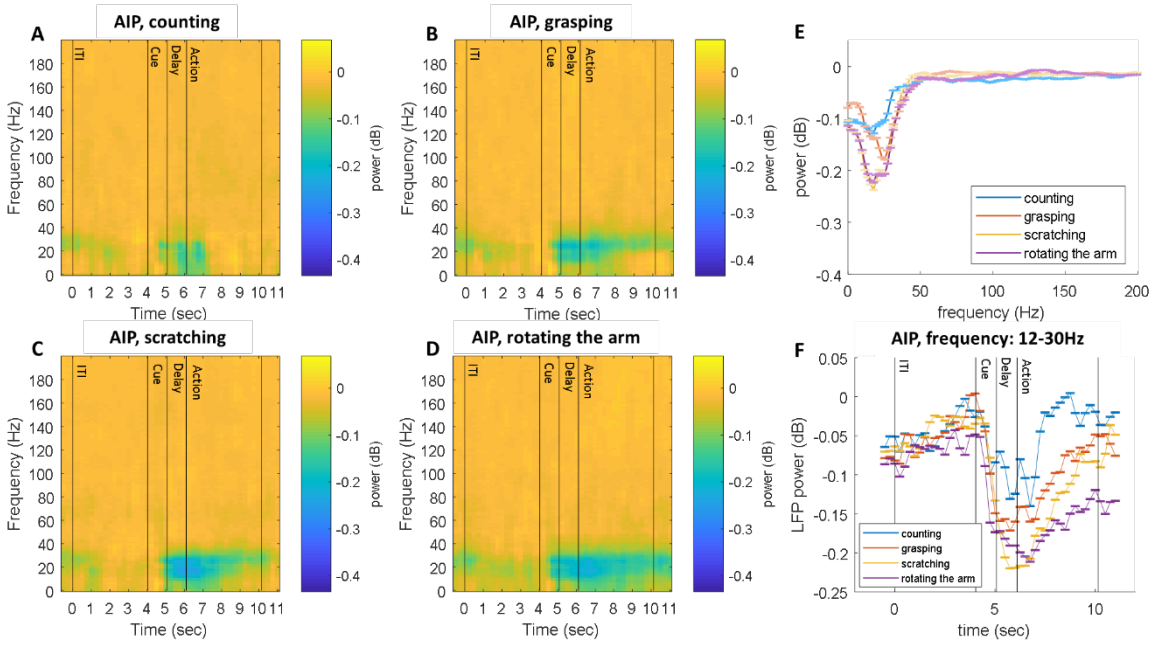

Figure S3. LFP power from AIP during action exploration task. A–D) Population-averaged spectrogram from AIP during counting (A), grasping (B), scratching (C), and rotating the arm (D). E) Average LFP power in the first one-second window in the action phase (population averaged). F) Temporal changes in average LFP power in 12–30Hz (population averaged).

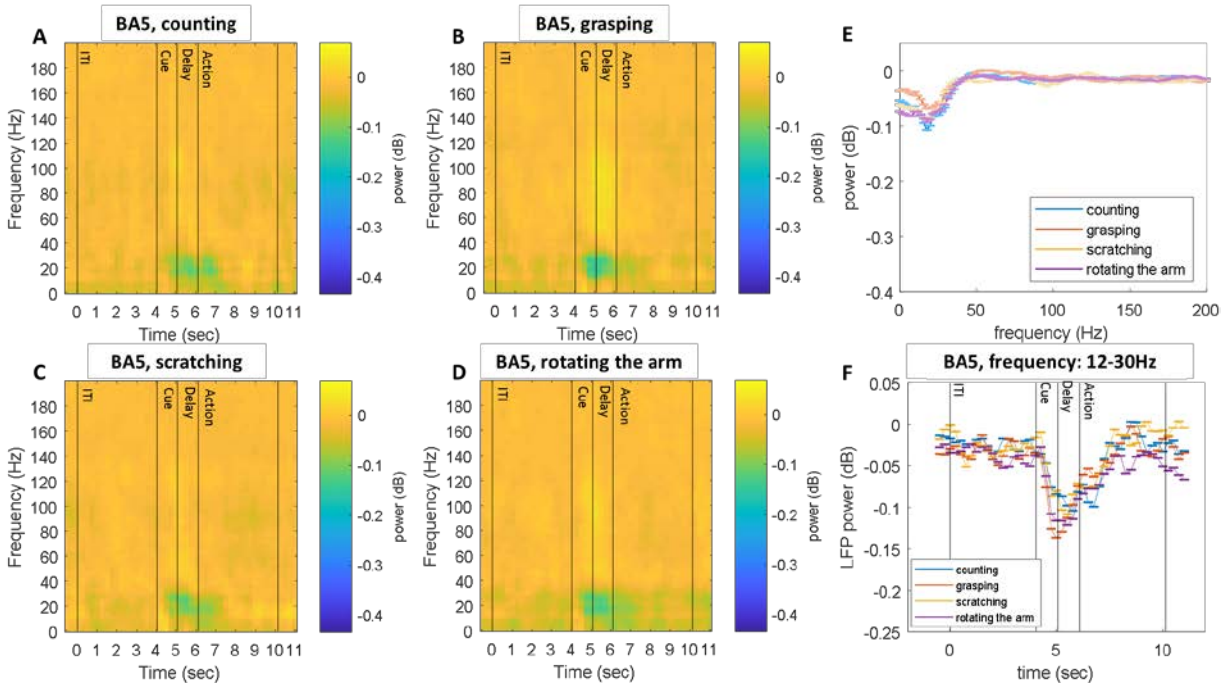

Figure S4. LFP power from BA5 during action exploration task. A-D) Population-averaged spectrogram from BA5 during counting (A), grasping (B), scratching (C), and rotating the arm (D). E) Average LFP power in the first one-second window in action phase (population averaged). F) Temporal changes in average LFP power in 12–30Hz (population averaged).

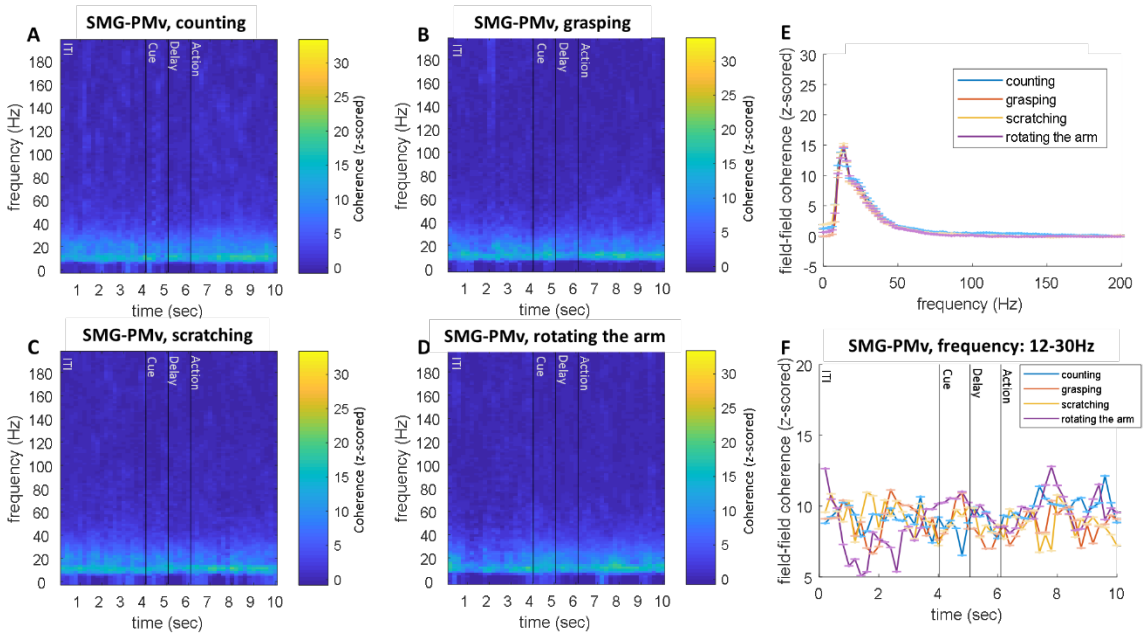

Figure S5. Field-field coherence between SMG and PMv during action exploration task. A–D) Population-averaged coherogram during counting (A), grasping (B), scratching (C), and rotating the arm (D). E) Average coherence in the first one-second window in the action phase (population averaged). The peak was observed at 16 Hz. F) Temporal changes in average coherence in 12–30Hz (population averaged). Every coherence value shown here is normalized.

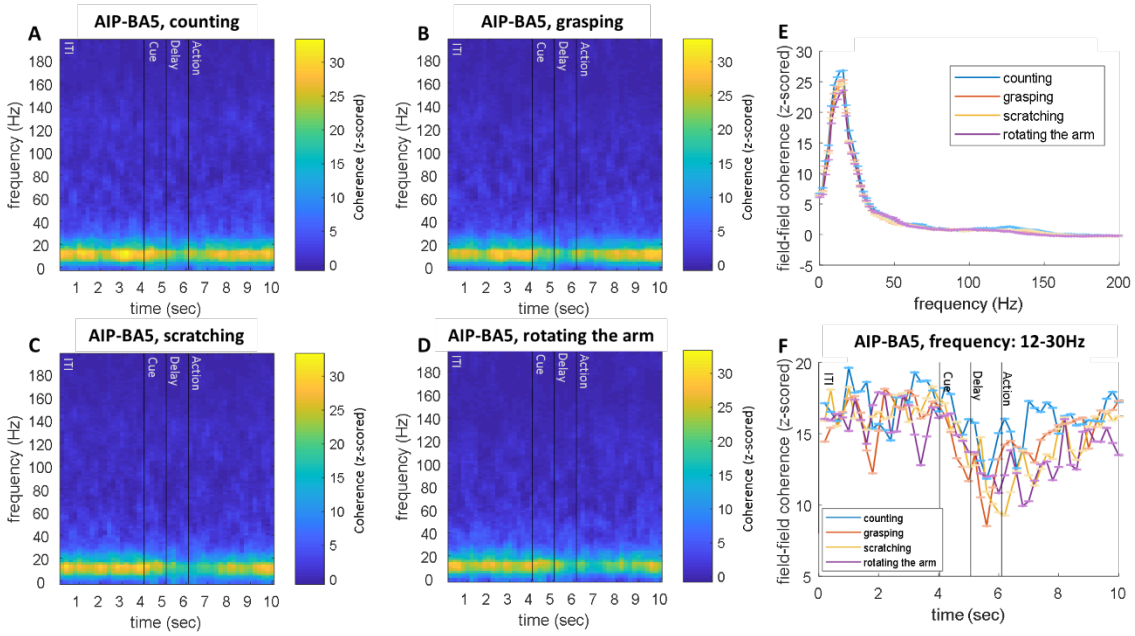

Figure S6. Field-field coherence between AIP and BA5 during action exploration task. A–D) Population-averaged coherogram during counting (A), grasping (B), scratching (C), and rotating the arm (D). E) Average coherence in the first one-second window in action phase (population averaged). The peak was observed at 14 Hz. F) Temporal changes in average coherence in 12–30Hz (population averaged). Every coherence value shown here is normalized.

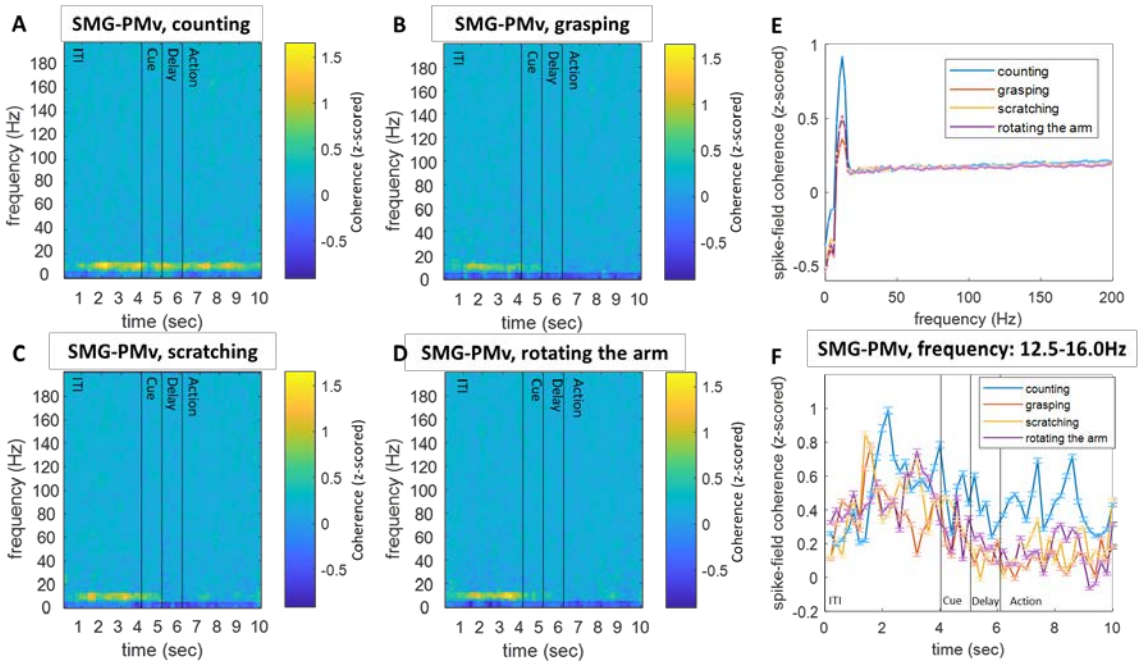

Figure S7. Spike-field coherence between SMG (spike) and PMv (LFP) during action exploration task. A–D) Population-averaged coherogram during counting (A), grasping (B), scratching (C), and rotating the arm (D). E) Average coherence in the first one-second window in the action phase (population averaged). F) Temporal changes in average coherence in 12–16Hz (population averaged). Every coherence value shown here is normalized.

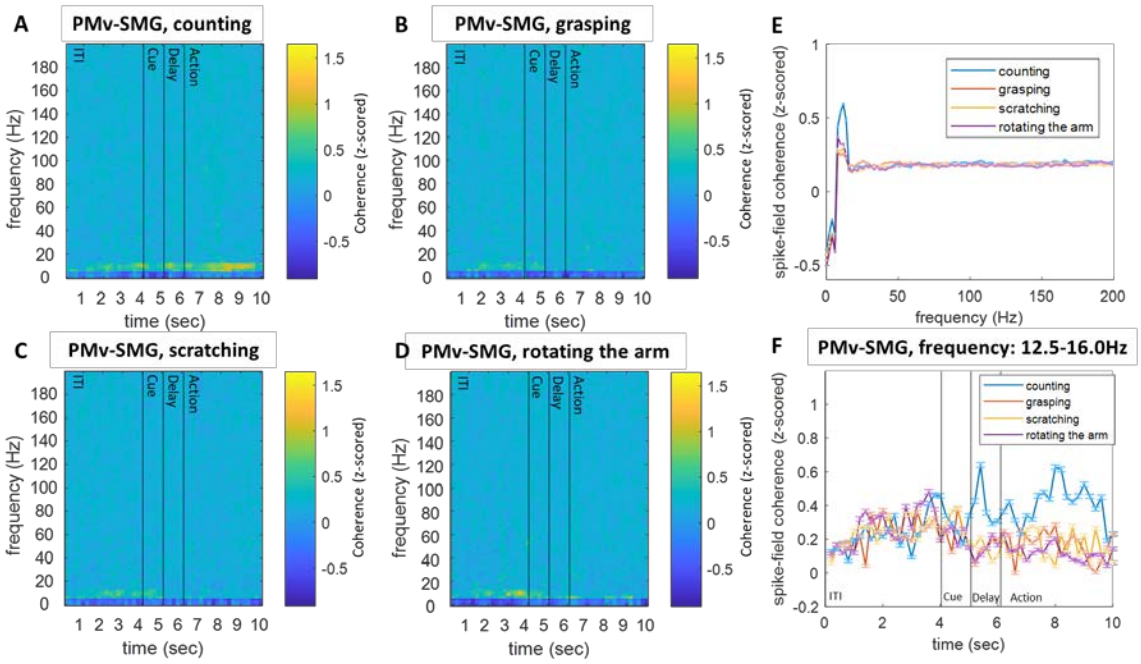

Figure S8. Spike-field coherence between PMv (spike) and SMG (LFP) during action exploration task. A–D) Population-averaged coherogram during counting (A), grasping (B), scratching (C), and rotating the arm (D). E) Average coherence in the first one-second window in action phase (population averaged). F) Temporal changes in average coherence in 12–16Hz (population averaged). Every coherence value shown here is normalized.